RESEARCH ARTICLE
ATMOSPHERIC PHYSICS

Earth and Planetary Physics
3: 166–181, 2019
doi: 10.26464/epp2019012

Evaluating the Brewer–Dobson circulation and its responses to ENSO, QBO, and the solar cycle in different reanalyses

Jian Rao[1,2,3*], YueYue Yu[1], Dong Guo[1], ChunHua Shi[1], Dan Chen[1], and DingZhu Hu[1]

[1]Key Laboratory of Meteorological Disaster, Ministry of Education (KLME)/Joint International Research Laboratory of Climate and Environment Change (ILCEC)/Collaborative Innovation Center on Forecast and Evaluation of Meteorological Disasters (CIC-FEMD), Nanjing University of Information Science & Technology, Nanjing 210044, China;

[2]State Key Laboratory of Numerical Modeling for Atmospheric Sciences and Geophysical Fluid Dynamics, Institute of Atmospheric Physics, Chinese Academy of Sciences, Beijing 100029, China;

[3]Fredy & Nadine Herrmann Institute of Earth Sciences, The Hebrew University of Jerusalem, Edmond J. Safra Campus, Givat Ram Jerusalem 91904, Israel

Abstract: This study compares the climatology and long-term trend of northern winter stratospheric residual mean meridional circulation (RMMC), as well as its responses to El Niño-Southern Oscillation (ENSO), stratospheric Quasi Biennial Oscillation (QBO), and solar cycle in ten reanalyses and a stratosphere-resolving model, CESM1-WACCM. The RMMC is a large-scale meridional circulation cell in the stratosphere, usually referred to as the estimate of the Brewer Dobson circulation (BDC). The distribution of the BDC is generally consistent among multiple reanalyses except that the NOAA twentieth century reanalysis (20RC) largely underestimates it. Most reanalyses (except ERA40 and ERA-Interim) show a strengthening trend for the BDC during 1979–2010. All reanalyses and CESM1-WACCM consistently reveal that the deep branch of the BDC is significantly enhanced in El Niño winters as more waves from the troposphere dissipate in the stratospheric polar vortex region. A secondary circulation cell is coupled to the temperature anomalies below the QBO easterly center at 50 hPa with tropical upwelling/cooling and midlatitude downwelling/warming, and similar secondary circulation cells also appear between 50–10 hPa and above 10 hPa to balance the temperature anomalies. The direct BDC response to QBO in the upper stratosphere creates a barrier near 30°N to prevent waves from propagating to midlatitudes, contributing to the weakening of the polar vortex. The shallow branch of the BDC in the lower stratosphere is intensified during solar minima, and the downwelling warms the Arctic lower stratosphere. The stratospheric responses to QBO and solar cycle in most reanalyses are generally consistent except in the two 20CRs.

Keywords: residual mean meridional stream function (RMMSF); Brewer-Dobson circulation (BDC); El Niño-Southern Oscillation (ENSO); Quasi-Biennial Oscillation (QBO)

Citation: Rao, J., Yu, Y. Y., Guo, D., Shi, C. H., Chen, D., and Hu, D. Z. (2019). Evaluating the Brewer–Dobson circulation and its responses to ENSO, QBO, and the solar cycle in different reanalyses. *Earth Planet. Phys.*, *3*(2), 166–181. http://doi.org/10.26464/epp2019012

1. Introduction

Since Brewer (1949) and Dobson and Massey (1956), it has increasingly been revealed that the stratospheric atmosphere and its trace gases are controlled by a large-scale meridional circulation, which ascends into the stratosphere from the tropics, and descends back to the troposphere in the extratropics. This meridional circulation is known as the Brewer-Dobson Circulation (BDC). The deep BDC branch is mainly forced by the extratropical wave activities, which transfer momentum preferentially against the vortex winds, thereby allowing a poleward flow. The troposphere-stratosphere coupling processes associated with the BDC modulate the mass exchange between them, and therefore the thermal and dynamical structures in the stratosphere and troposphere are changed, redistributing the water vapor, ozone, and other traces (Roscoe, 2006).

This troposphere–stratosphere mass exchange is mainly controlled by the BDC, expressed as the net upward mass flux in the tropics (Holton, 1990). The transformed Eulerian-mean (TEM) equation (Andrews et al., 1987) can be used to compute the residual mean meridional stream function (RMMSF). The BDC is an overall stratospheric transport system, and the RMMSF in the stratosphere is a good metric of the BDC. According to "the downward control principle" proposed by Haynes et al. (1991), the meridional flow is driven by the wave forcing in the middle latitudes associated with the breakdown and dissipation of the upward propagating gravity and Rossby waves, whose sources are primarily located in the troposphere (Plumb, 2002; Shepherd, 2007). These investigators also suggest the importance of synoptic waves in the lower stratosphere and importance of the gravity waves in the mesosphere. The upward (downward) mass flux in the tropics (extratropics) varies with season, and the maximum mass flux value appears in the northern winter (e.g., Holton, 1990;

Correspondence to: J. Rao, raojian@nuist.edu.cn
Received 04 NOV 2018; Accepted 18 JAN 2019.
Accepted article online 25 FEB 2019.

Rosenlof and Holton, 1993; Rosenlof, 1995; Wang WG et al., 2015). By calculating the residual circulation trajectory in the latitude-altitude plane, Birner and Bönisch (2011) showed that the BDC consists of a deep branch related to the planetary wave breaking in the mid-to-upper stratosphere and a shallow branch related to the wave breaking in the subtropical lower stratosphere.

The BDC is important to atmospheric chemistry because it carries ozone-depleting gases such as CFCs and N_2O into the stratosphere on one hand, and also brings ozone down into the troposphere, supplying a substantial proportion of the ozone in the troposphere in the absence of pollution (Forster and Shine, 1999; Lubis et al., 2017; de la Cámara et al., 2018). For example, using a reanalysis and model simulations, Lubis et al. (2017) found that enhanced upward wave flux can be absorbed in the extratropical stratosphere to speed up the BDC, leading to an increase in the polar stratospheric ozone, while downward wave reflection is related to lower polar stratospheric ozone concentration. Changes in the BDC are also associated with the concentrations of some trace gases like NO_2, N_2O, H_2O and CO_2 (Roscoe, 2006; Engel et al., 2008; Calvo et al., 2010). The strength of the stratospheric polar vortex associated with the BDC also affects surface pressure, winds, and temperatures in winter (Polvani and Kushner, 2002; Baldwin et al., 2003).

On the interannual timescale, it was revealed that the BDC was enhanced in the 1970s, but weakened in the 1990s, which was intimately associated with changes in the concentrations of some trace gases like NO_2, N_2O, H_2O and CO_2 (Roscoe, 2006). By adopting a reanalysis from the European Centre for Medium Range Weather Forecasts (ECMWF) and integrating vertically the residual meridional velocity, Seviour et al. (2012) revealed that the BDC and the upward mass flux in the tropics have decreased in the most recent two decades. As the earth surface is warming, some models have indicated a strengthening of the BDC (Rind et al., 1990; Butchart et al., 2006, 2010; Garcia and Randel, 2008; McLandress and Shepherd, 2009; Butchart, 2014). It is generally expected that an increase in greenhouse gases (GHGs) modifies the radiative balance to cause warming in the troposphere and cooling in the stratosphere. A change in temperature also induces a change in the background wind field through the thermal wind balance, leading to a change of the wave forcings as well (Garcia and Randel, 2008; McLandress and Shepherd, 2009). An increase in GHG concentrations induces increasing wave dissipation in the stratosphere (Lubis et al., 2018a) and a strengthened stratospheric residual circulation, as well as a lifting of the entire atmospheric circulation in response to future GHGs (Garcia and Randel, 2008; Oberländer-Hayn et al., 2016). Recent studies have shown that both GHGs and ozone-depletion can induce changes in the BDC (e.g., Lossow et al., 2012, Lubis et al., 2016; Polvani et al., 2018). The ozone depletion in the Southern Hemisphere led to enhanced stratospheric residual circulation in the austral spring and its effect was coupled vertically to the residual circulation in the mesosphere and lower thermosphere (e.g., Lossow et al., 2012, Lubis et al., 2016). Polvani et al. (2018) also found that increasing ozone depleting substances partially explain the BDC trend in the late twentieth century. However, the BDC trend has not been found in the relatively short observation records (Engel et al., 2008) and a growing interest is placed in the historical reanalysis datasets.

The assessment of the BDC in some reanalyses has been reported in recent studies (Iwasaki et al., 2009; Seviour et al., 2012; Abalos et al., 2015; Wang WG, 2015; Miyazaki et al., 2016), as well as its responses to the El Niño-Southern Oscillation (ENSO; Randel et al., 2009; Calvo et al., 2010; Simpson et al., 2011; Abalos et al., 2015), stratospheric Quasi Biennial Oscillation (QBO; White et al., 2015; Abalos et al., 2015; Rao J and Ren RC, 2017, 2018), and solar cycle (Kodera and Kuroda, 2002; Gray et al., 2004; Matthes et al., 2006; Camp and Tung, 2007; Rind et al., 2008). Iwasaki et al. (2009) found that the interannual variability of the BDC in winter is coincident among five selected reanalyses, but the yearly trends are inconsistent. Abalos et al. (2015) used three estimates of the BDC for three modern reanalyses and also found substantial uncertainty in the mean BDC magnitude. Based on mass-weighted isentropic zonal means, Miyazaki et al. (2016) also revealed large discrepancies between different meteorological variables and their trends in different reanalyses. However, the enhanced BDC in El Niño winters relative to La Niña winters, in easterly QBO phases relative to westerly QBO phases, and during solar minima relative to solar maxima, are consistently observed and modeled (Gray et al., 2004; Rind et al., 2008; Randel et al., 2009; Calvo et al., 2010; Simpson et al., 2011; White et al., 2015; Abalos et al., 2015; Rao J and Ren RC, 2018).

The RMMSF is not a standard output for reanalysis datasets; this study is aimed to present the winter mean BDC diagnosed from daily outputs of more reanalyses than in Iwasaki et al. (2009) and Abalos et al. (2015). Therefore, a more comprehensive comparison of ten reanalyses is provided in this study for the interannual variability of the BDC and its responses to ENSO, QBO, and solar cycle. We mainly focus on the northern winter season, because the northern stratospheric responses to ENSO, QBO, and solar cycle, as well as the stratosphere-troposphere coupling, are strongest in this season. The BDC derived from a fully coupled model historical run forced by all forcings (GHGs, ozone depletion, QBO, and solar cycle) is also shown, in order to test the consistency between reanalyses and model simulations. The organization of the paper is as follows. Section 2 gives a brief description of data and methodology about the BDC calculation. A parallel comparison of the northern winter BDC climatology in multiple datasets is displayed in Section 3. The time series of the tropical vertical mass flux across 100 hPa and 70 hPa is derived from each reanalysis and shown in Section 4. We check, in Section 5, the consistencies between the BDC by comparing their responses to ENSO, QBO, and solar cycle in each reanalysis. Our results are summarized in Section 6.

2. Data and Methodology

2.1 Data

We quantify the BDC diagnosed from the ten available reanalyses listed in Table 1, including CFSR (Saha et al., 2010), ERA40 (Uppala et al., 2005), ERAIN (Dee et al., 2011), JRA25 (Onogi et al., 2007), JRA55 (Ebita et al., 2010), MERRA (Rienecker et al., 2011), NCEP1 (Kalnay et al., 1996), NCEP2 (Kanamitsu et al., 2002), ECMWF's

20CR (Hersbach et al., 2015), and NOAA's 20CR (Compo et al., 2011). See Table 1 for their full names and refer to the SPARC Reanalysis Intercomparison Project for more details (Fujiwara et al., 2017). Most reanalyses, including ERA40, ERAIN, JRA25, NCEP1, NCEP2, and 20CR-NOAA have been used to assess the polar vortex oscillation events in Rao J et al. (2015). In this study, CFSR, JRA55, MERRA, and 20CR-ECMWF are also included to make a relatively more comprehensive comparison between BDCs in ten datasets. More information about the spatial resolution, vertical level number, and references are provided in Table 1. We also use the Hadley Centre Sea Ice and Sea Surface Temperature (SST) dataset (Rayner et al., 2003) to select ENSO events. The CESM1-WACCM is a fully coupled earth system model with a stratosphere-solving atmosphere, which has been widely used to study the atmospheric response to SST forcing (Xie F et al., 2012; Ren RC et al., 2017; Rao J and Ren RC, 2018). The CESM1-WACCM historical free-running simulation was performed with all observed forcings from 1850 to 2005. The model includes interactive chemistry, ocean, land, and sea ice. The observed forcings include changes in surface concentrations of radiatively active species, daily solar spectral irradiance, volcanic sulfate heating, and the QBO (Marsh et al., 2013). The daily outputs of the historical run by CESM1-WACCM are diagnosed.

2.2 Residual Mean Meridional Stream Function

In log-pressure coordinates, the TEM residual velocities are defined as

$$\bar{v}^* = \bar{v} - \frac{1}{\rho_0}\frac{\partial}{\partial z}\left(\rho_0\overline{v'\theta'}/\overline{\theta}_z\right),\quad \bar{w}^* = \bar{w} + \frac{1}{a\cos\varphi}\frac{\partial}{\partial\varphi}\left(\cos\varphi\overline{v'\theta'}/\overline{\theta}_z\right), \tag{1}$$

where an overbar represents a zonal mean, and all other terms are also identically defined by Andrews et al. (1987). In spherical log-pressure coordinates the TEM form continuity equation is expressed as

$$\frac{1}{a\cos\varphi}\frac{\partial}{\partial\varphi}(\bar{v}^*\cos\varphi) + \frac{1}{\rho_0}\frac{\partial}{\partial z}(\rho_0\bar{w}^*) = 0, \tag{2}$$

where $\bar{v}^*$ and $\bar{w}^*$ are the meridional and vertical components of the residual velocity; a is the radius of the Earth; φ is the latitude; z is the log-pressure height ($z = -H\log\frac{p}{1000\ \mathrm{hPa}}$, p is the pressure, H=7000 m); ρ_0 is the air density. For the non-divergent type of movement in equation (2), the RMMSF (Ψ^*) can be defined as

$$\bar{v}^* = -\frac{1}{\rho_0\cos\varphi}\frac{\partial\Psi^*}{\partial z}, \bar{w}^* = \frac{1}{\rho_0 a\cos\varphi}\frac{\partial\Psi^*}{\partial\varphi}. \tag{3}$$

With the boundary conditions that $\varphi\to 90°\mathrm{N}$, $\Psi^*\to 0$, and $p\to 0$ ($z\to\infty$), $\Psi^*\to 0$, the RMMSF can be obtained by integrating vertically meridional velocity in equation (3):

$$\Psi^* = \int_z^\infty \rho_0\bar{v}^*\cos\varphi\mathrm{d}z. \tag{4}$$

Substituting equation (1) into equation (4), we obtain the formula as below.

$$\begin{aligned}\Psi^* &= \int_z^\infty \rho_0\left[\bar{v} - \frac{1}{\rho_0}\frac{\partial}{\partial z}\frac{\rho_0\overline{v'\theta'}}{\overline{\theta}_z}\right]\cos\varphi\mathrm{d}z\\ &= \int_z^\infty \rho_0\bar{v}\cos\varphi\mathrm{d}z + \frac{\rho_0\overline{v'\theta'}}{\overline{\theta}_z}\cos\varphi.\end{aligned} \tag{5}$$

The difference of the RMMSF at the turnaround latitudes ($\Psi^*_{\max} - \Psi^*_{\min}$) in both hemispheres can be used to measure the vertical mass flux in the tropics (Holton, 1990). The northern (southern) turnaround latitude is near 20°N (25°S), so the total vertical mass flux can be also measured by RMMSF difference between two specific latitude bands ($\Psi^*_{15-25°\mathrm{N}} - \Psi^*_{20-30°\mathrm{S}}$). We also use the Eliassen-Palm (EP) flux (F_y, F_z) and its divergence to diagnose the wave propagation and dissipation (Andrews et al.,

Table 1. Ten reanalyses compared in this study

Dataset	Dataset expansion	Spatial resolution	Level No.	Reference
CFSR	National Centers for Environmental Prediction's Climate Forecast System Reanalysis	0.5×0.5	37	Saha et al., 2010
ERA40	European Centre for Medium-Range Weather Forecasts 40 Years Reanalysis	2.5×2.5	23	Uppala et al., 2005
ERAIN	European Centre for Medium-Range Weather Forecasts Interim Reanalysis	1.5×1.5	37	Dee et al., 2011
JRA25	Japanese 25-year Reanalysis	1.25×1.25	23	Onogi et al., 2007
JRA55	Japanese 55-year Reanalysis	1.25×1.25	37	Ebita et al., 2010
MERRA	National Aeronautics and Space Administration's Modern-Era Retrospective Analysis for Research and Applications	1.25×1.25	42	Rienecker et al., 2011
NCEP1	National Centers for Environmental Prediction–National Center for Atmospheric Research Reanalysis I	2.5×2.5	17	Kalnay et al., 1996
NCEP2	National Centers for Environmental Prediction–U.S. Department of Energy Reanalysis II	2.5×2.5	17	Kanamitsu et al., 2002
20CR-ECMWF	ECMWF's Atmospheric Reanalysis of the 20th Century	2.5×2.5	37	Hersbach et al., 2015
20CR-NOAA	NOAA Twentieth-Century Reanalysis Project, version 2	2.0×2.0	24	Compo et al., 2011

1987).

3. A Parallel Comparison of the Northern Winter BDC Climatology in Reanalyses

Figure 1 presents the long-term mean of the Northern Hemisphere winter (December, January, and February, DJF) BDC from ten reanalyses and CESM1-WACCM, respectively, which is extracted from 1979–2002 for ERA40, from 1979–2010 for other reanalyses, and from 1979–2005 for CESM1-WACCM. Different reanalyses consistently reveal that the Northern Hemisphere BDC develops much deeper than the Southern Hemisphere counterpart during the northern winter. In particular, the deep branch of the BDC is a large-scale meridional circulation which ascends in the tropics, equatorward of 20° in both hemispheres, and descends in the extratropics, poleward of 25° above 100 hPa. The northern turnaround latitude is near 20°N, while the southern turnaround latitude is near 25°S. The general pattern of the RMMSF in the stratosphere is consistent among the reanalyses and CESM1-WACCM. The stratospheric RMMSF in 20CR-NOAA is largely underestimated due to the lack of a resolved stratosphere in the model, whereas the hemispheric circulation cell in 20CR-ECMWF seems to be more realistic.

Figure 2 presents the RMMSF climatology at 100 hPa and 70 hPa from the reanalyses and CESM1-WACCM. It can be seen that the northern turnaround latitude and intensity of the BDC vary with dataset and height. The 100-hPa BDC from ERA40, NCEP1, and NCEP2 turns around near 10°N–15°N, while that from other reanalyses turns around near 20°N–30°N, consistent with Fig.2 in Iwasaki et al. (2009) and Fig.2 in Abalos et al. (2015). The turnaround latitude (20°N–25°N) at 70 hPa is much more uniform among different reanalyses than that at 100 hPa. However, the southern turnaround latitude is near 30°S, consistent among the datasets. The RMMSF difference between the turnaround latitudes in the Northern and Southern Hemispheres ($\Psi_{\max} - \Psi_{\min}$) denotes the vertical mass flux in the tropics. The climatology of the tropical vertical mass flux at 100 hPa and 70 hPa is given in Table 2. The tropical vertical mass flux has a large inter-reanalysis range from 2.12×10^{10} kg/s in CFSR to 4.43×10^{10} kg/s in ERA40 at 100 hPa. The reanalysis ensemble mean is 2.91×10^{10} kg/s at 100 hPa (not shown), close to the vertical mass flux in CESM1-WACCM, 2.79×10^{10} kg/s and the reanalysis median, 2.76×10^{10} kg/s (ERAIN). Similarly, the vertical mass flux at 70 hPa ranges from 0.79×10^{10} kg/s in 20CR-NOAA to 1.64×10^{10} kg/s in ERA40 with a reanalysis ensemble mean, 1.24×10^{10} kg/s (not shown), which is also consistent with CESM1-WACCM, 1.13×10^{10} kg/s. Compared with the reanalysis ensemble mean and CESM1-WACCM, the BDC is relatively weak in CFSR, MERRA, 20CR-ECMWF, and 20CR-NOAA, and it is overestimated in ERA40. We also used the RMMSF difference in two latitude bands (i.e., 15°N–25°N and 20°S–30°S) to represent the vertical mass flux in the tropics and found the conclusions are robust (not shown).

4. Changes of the Northern Hemisphere Winter BDC

The northern (southern) extratropical total downward mass flux can be assessed by the maximum (minimum) RMMSF at 100 hPa

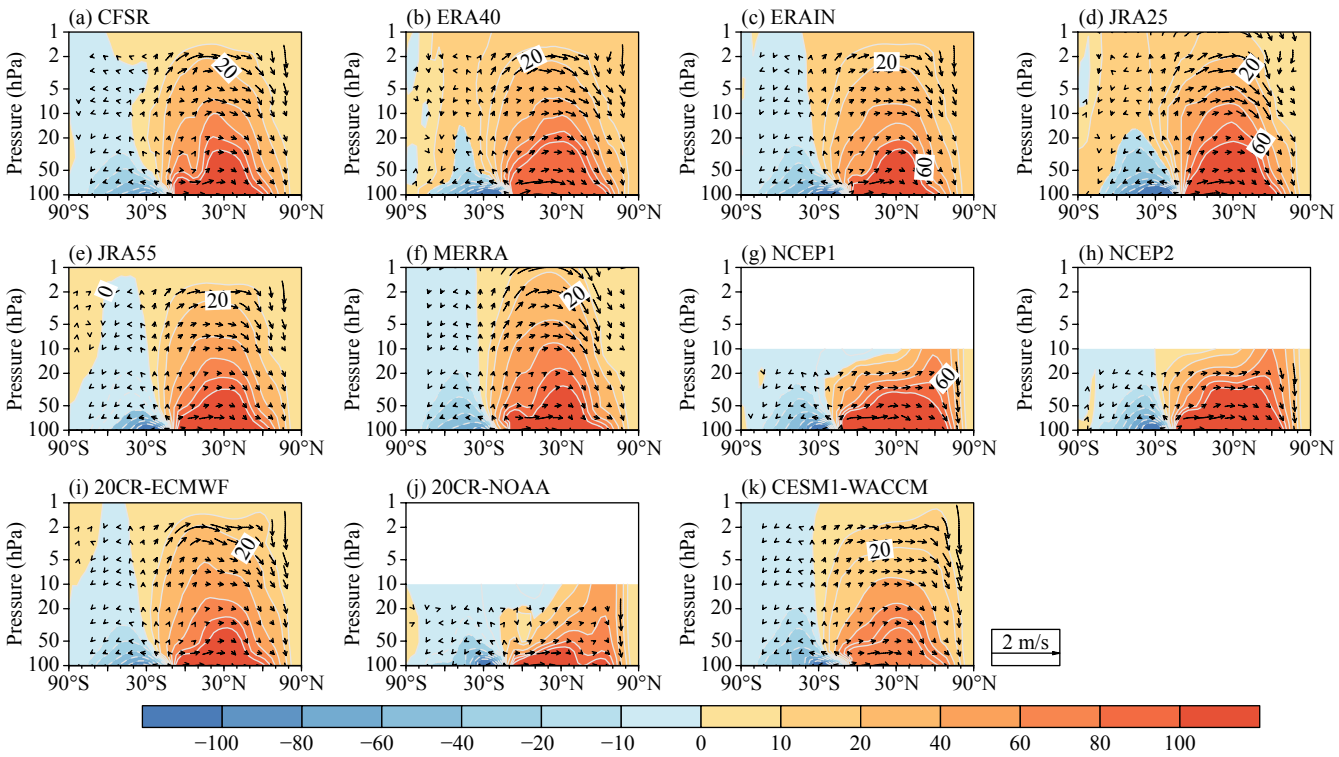

Figure 1. The climatology of the northern winter (December-January-February, DJF) RMMSF (1979–2002 for ERA40, and 1979–2010 for other reanalyses) in the stratosphere (units: kg/m/s) from ten reanalyses and CESM1-WACCM, respectively. The vectors show the scaled residual velocity ($\bar{v}^*, 250\times\bar{w}^*$; units: m/s).

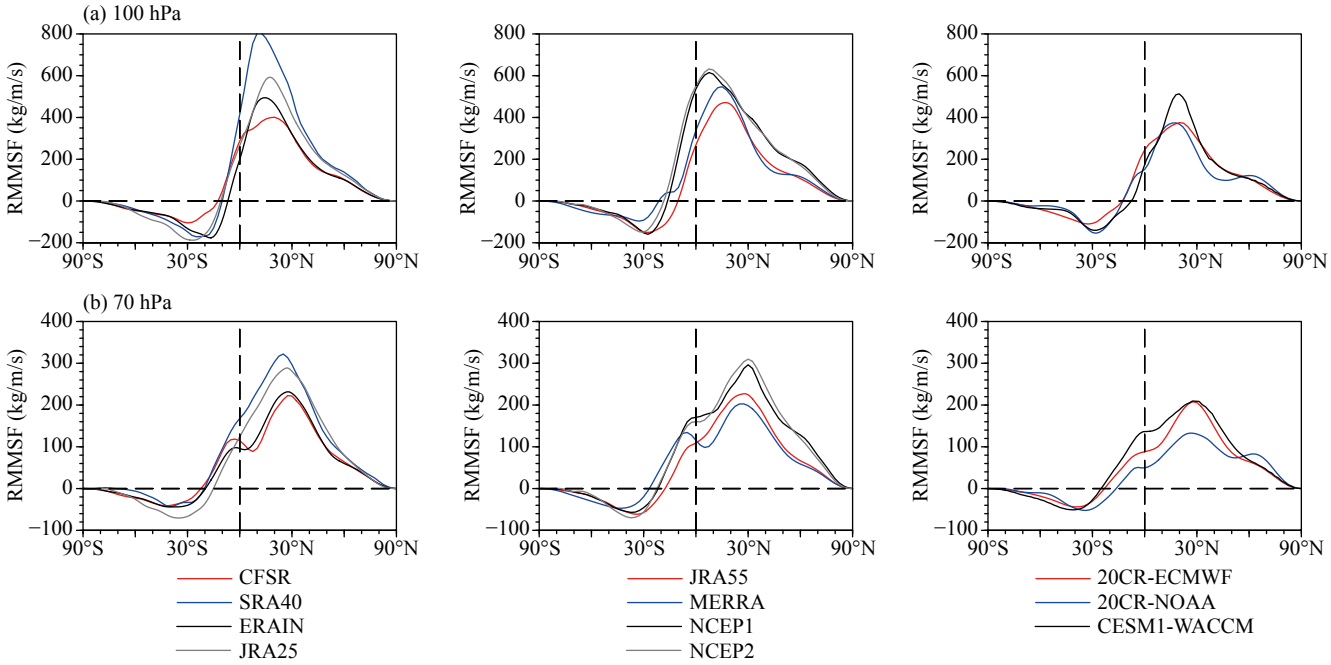

Figure 2. The climatology of the northern winter RMMSF (1979–2002 for ERA40, and 1979–2010 for other reanalyses) at (a) 100 hPa and (b) 70 hPa (units: kg/m/s) from ten reanalyses and CESM1-WACCM, respectively.

Table 2. The climatology of the vertical mass flux in the tropics at 100 hPa and 70 hPa ($2\pi a \times (\Psi^*_{\max} - \Psi^*_{\min})$); units: 10^{10} kg/s)

Dataset	100 hPa	70 hPa
CFSR	2.12	1.08
ERA40	4.43	1.64
ERAIN	2.76	1.12
JRA25	3.16	1.45
JRA55	2.63	1.20
MERRA	2.65	1.00
NCEP1	3.77	1.51
NCEP2	3.14	1.53
20CR-ECMWF	2.14	1.08
20CR-NOAA	2.34	0.79
CESM1-WACCM	2.79	1.13

or 70 hPa (Holton, 1990; Wang WG et al., 2015), across which the vertical component of the residual velocity changes sign. In a BDC cell, net downward mass flux is observed in the extratropical stratosphere, measured by the RMMSF at the turnaround latitude. The tropical vertical mass flux in the tropics is assessed using the RMMSF difference near the turnaround latitudes in both hemispheres, $\Psi^*_{\max} - \Psi^*_{\min}$. Time series of the tropical vertical mass flux during the northern winter at 100 hPa and 70 hPa is shown in Figures 3 and 4.

The interannual variability of the tropical vertical mass flux at 100 hPa is different among the reanalyses. In other words, the interannual variation of the BDC is quite sensitive to the choice of reanalyses and has a large uncertainty among datasets. In particular, the variability of the mass flux in ERA40 and ERAIN is larger than in other reanalyses (Figure 3). The interannual variability of the BDC in 20CR-ECMWF and 20CR-NOAA is relatively smaller than other reanalyses (see the ordinate value ranges). Similarly, the interannual variation amplitude of the vertical mass flux at 70 hPa is nearly identical in Figures 4a–h, and the two 20CRs (Figures 4i, j) are consistent with other reanalyses for some extreme BDC winters (strong BDC: 1990, 1998, 2009; weak BDC: 1980, 1988, 1992, 1999).

The linear trend of the tropical upward mass flux is also shown for each reanalysis during 1979–2010 (gray lines) in Figures 3 and 4. The decreasing trend of the BDC in ERA40 and ERAIN has been reported in recent studies (Fig. 3 in Iwasaki et al. (2009), Fig. 9 in Seviour et al. (2012); Fig. 14 in Abalos et al. (2015), Fig. 2 in Wang WG et al. (2015), and Fig. 5 in Miyazaki et al. (2016)), which is also confirmed at 100 hPa and 70 hPa (Figures 3c, 4c). Specifically, the linear trend of the tropical upward mass flux at 100 hPa in ERAIN is -2.61×10^8 kg/s/yr, which is above the 95% confidence level according to the Student's *t*-test. However, the linear trend of the tropical upward mass flux varies with the datasets, as shown in Table 3. A slightly increasing trend of the BDC during 1979–2010 is found in most reanalyses, even above the 95% confidence level in CFSR, JRA25, NCEP1, and NCEP2. Therefore, the BDC trend inferred from the reanalyses has large uncertainty. Iwasaki et al. (2009) also found that the yearly trends for the BDC are not reliably observed due to large diversity among the reanalyses, and Abalos et al. (2015) identified a strengthening of tropical upwelling from 100–10 hPa in JRA55 and MERRA when the reanalyses were extended to 2012. Consistent with the previous studies, the CESM1-WACCM also shows an increasing trend of the BDC. The deep branch of the BDC is mainly forced by extratropical wave activities, which shows a weak linear trend in both obser-

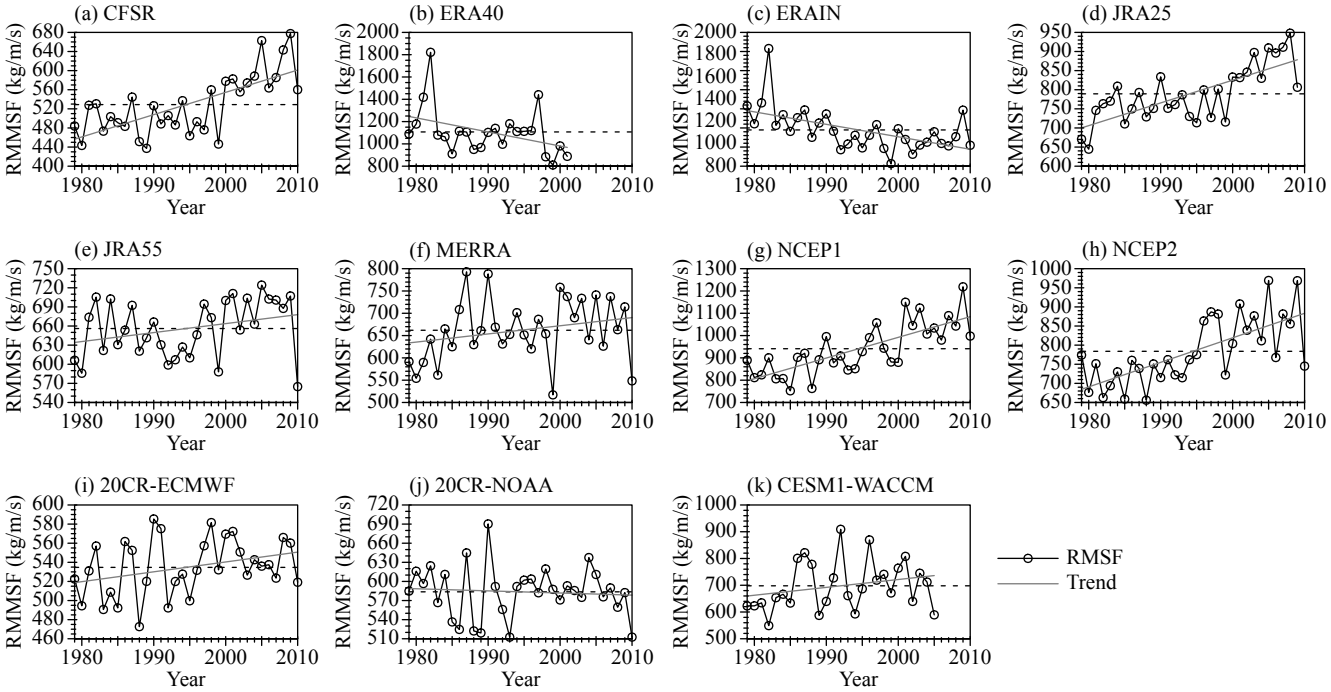

Figure 3. Time series of the tropical vertical mass flux ($\Psi^*_{\max} - \Psi^*_{\min}$; units: kg/m/s) in the northern winter at 100 hPa (see context). The gray line presents the time trend since 1979. The horizontal dashed line denotes the climatology.

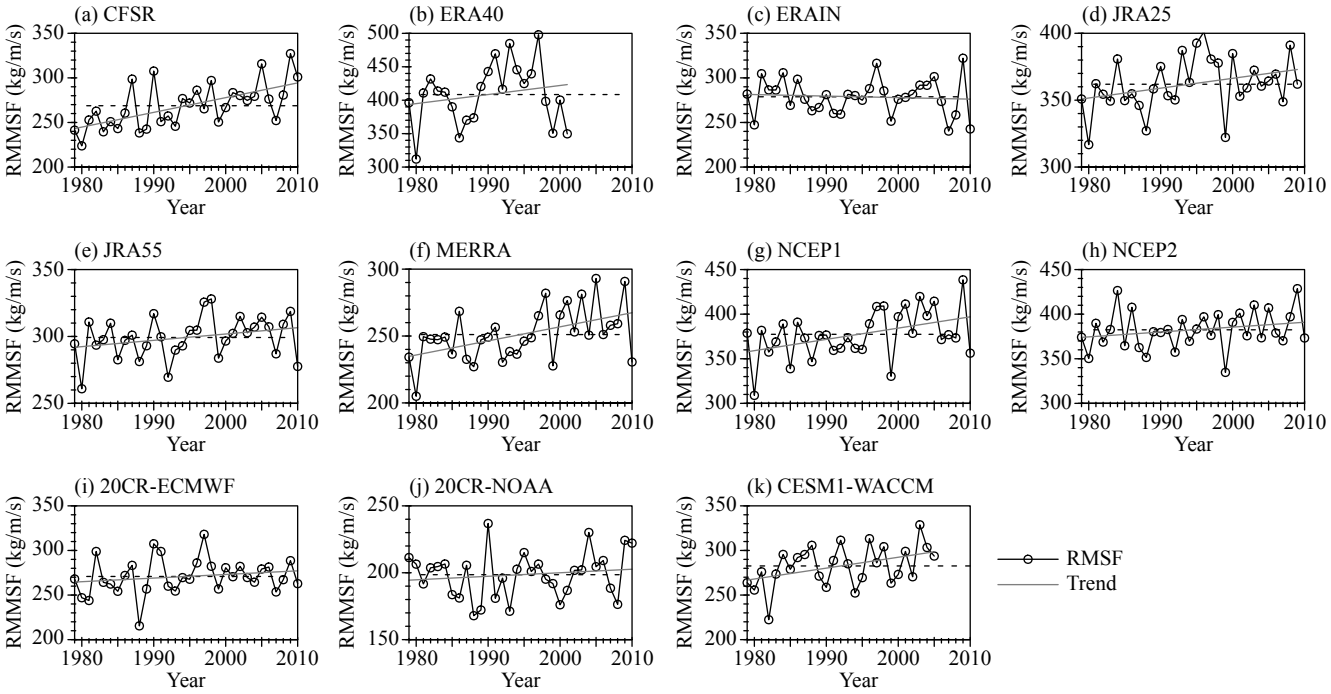

Figure 4. As in Figure 3 but for time series of the tropical vertical mass flux in the northern winter at 70 hPa.

vations and models (Hu YY and Tung, 2002; Rao J et al., 2015). Consistent with the BDC trend, the EP flux divergence shows a negative trend in the extratropical stratosphere in most reanalyses, while the EP flux divergence in the mid-stratosphere shows a positive trend 30°N of poleward in ERAIN (not shown).

5. BDC Responses to ENSO, QBO, and Solar Cycle

To assess the BDC comprehensively from different datasets, the composite responses to ENSO, QBO, and solar cycle are also compared among the reanalyses and CESM1-WACCM after the trends are removed for the BDC and other variables. The El Niño event is selected when the winter mean Niño3.4 (5°S–5°N, 170°–120°W) index is above 1.0 standard deviation, and the Niña event is selected when the winter mean Niño3.4 index is below −1.0 standard

Table 3. The time trend of the vertical mass flux in the tropics at 100 hPa and 70 hPa (units: 10^8 kg/s/yr). The single asterisk marks the trend above the 90% confidence level, and the double asterisks mark the trend above the 95% confidence level

Dataset	100 hPa	70 hPa
CFSR	1.87**	0.66**
ERA40	–5.06*	0.54*
ERAIN	–2.61**	–0.07
JRA25	2.38**	0.29*
JRA55	0.56	0.19
MERRA	0.73	0.42**
NCEP1	3.71**	0.51**
NCEP2	2.57**	0.22
20CR-ECMWF	0.41	0.16
20CR-NOAA	–0.13	0.11
CESM1-WACCM	1.18	0.49**

deviation. We also change the threshold from ±1.0 to ±0.5 standard deviations, but the composite BDC response patterns are similar between the two criteria, although the response amplitude using the ±0.5 standard deviation is smaller for every reanalysis and CESM1-WACCM. The QBO index is defined as the equatorial (5°S–5°N) zonal mean zonal wind at 50 hPa (White et al., 2015; Rao J and Ren RC, 2017, 2018). Considering the asymmetry of the QBO westerlies and easterlies, all years are ranked according to the equatorial zonal mean zonal wind amplitudes. Nearly one third of years from 1970–2010 are selected as the QBO westerly years, one third as the QBO easterly years, and the other one third as the QBO neutral years. Namely, the nine strongest westerly years are selected as the westerly QBO events; and the nine strongest easterly years are selected as the easterly QBO events. The maximum solar years are selected when the winter solar flux 10.7 cm is above 1.0 standard deviation, and the minimum solar years are selected when the solar flux is below –1.0 standard deviation. The composite BDC difference between solar maxima and solar minima are also insensitive to the criteria if we change the threshold between 0.5 and 1.5 standard deviations. The extreme events for ENSO, QBO, and solar cycle are shown in Table 4.

5.1 ENSO

The stratospheric temperature response to ENSO during Northern Hemisphere winter has been widely explored in previous studies (e.g., Wei K et al., 2007; Garfinkel and Hartmann, 2008; Randel et al., 2009; Calvo et al., 2010; Simpson et al., 2011; Xie F et al., 2012; Rao J and Ren RC, 2016a, b, c, 2018; Hu JG et al., 2017; Ren RC et al., 2017). Abalos et al. (2015) found that a large portion of the yearly BDC variance is related to the contribution by ENSO. The composite differences in the residual velocity and the zonal-mean temperature between El Niño and La Niña winters are shown in Figure 5 for the ten reanalyses and CESM1-WACCM. As reported in previous studies, warm SST anomalies associated with El Niño enhance the convection in the tropical Pacific, which further excites a positive Pacific-North America (PNA)-like pattern in the extratropical troposphere. A positive PNA-like height pattern intensifies the climatological planetary waves, which can propagate upward into the stratosphere, favoring a disturbed stratospheric polar vortex. Reanalyses and CESM1-WACCM also consistently reveal that the weak and warm stratospheric polar vortex in El Niño winters can be explained by the enhanced BDC. Relative to observations during La Niña winters, the vertical component of the residual velocity during El Niño winters is positive in the tropical stratosphere from 100 hPa to 1 hPa in all reanalyses and CESM1-WACCM, implying that the equatorial upwelling is strengthened (Randel et al., 2009; Calvo et al., 2010). The uniform enhancement of the vertical motion in the tropical stratosphere is consistent with the cold temperature anomalies there. The strengthened BDC corresponds to an intensified downwelling in the extratropics, favoring a weak and warm polar vortex through adiabatic heating associated with downwelling.

The intensified BDC in the Northern Hemisphere during El Niño winters is consistently revealed by all reanalyses and CESM1-WACCM. The significant temperature response appears mainly in the Arctic stratosphere and the maximum temperature response is 7 K in most reanalyses. The stratospheric polar vortex response to ENSO in 20CR-ECMWF is the strongest (12 K) among the ten reanalyses, which is consistent with the strongest downwelling response in the Arctic stratosphere. The significant warm response related to the enhanced downwelling of the BDC over the Arctic during El Niño is also seen in 20CR-NOAA, although the warm temperature response center is shifted to mid-to-high latitudes and the downwelling is narrow.

Figure 6 shows the composite differences in the zonal-mean zonal wind, the EP flux, and its divergence between El Niño and La Niña winters, from reanalyses and CESM1-WACCM to explain the BDC responses via the enhanced dissipation and absorption of waves in the stratosphere (Plumb, 2002; Shepherd, 2007; Rao J

Table 4. Extreme events for ENSO, QBO and solar cycle during 1979–2010

Extreme events		Winters
ENSO	El Niño	1982/83, 1991/92, 1997/98, 2002/03, 2006/07, 2009/10
	La Niña	1984/85, 1988/89, 1998/99, 1999/00, 2007/08
QBO (50 hPa)	Westerly	1980/81, 1982/83, 1985/86, 1988/89, 1990/91, 1999/00, 2004/05, 2006/07, 2008/09
	Easterly	1979/80, 1984/85, 1989/90, 1996/97, 1998/99, 2001/02, 2003/04, 2005/06, 2007/08
Solar Cycle	Maximum	1979/80, 1980/81, 1981/82, 1988/89, 1989/90, 1990/91, 1991/92, 2001/02
	Minimum	1984/85, 1986/87, 1995/96, 1996/97, 2007/08, 2008/09

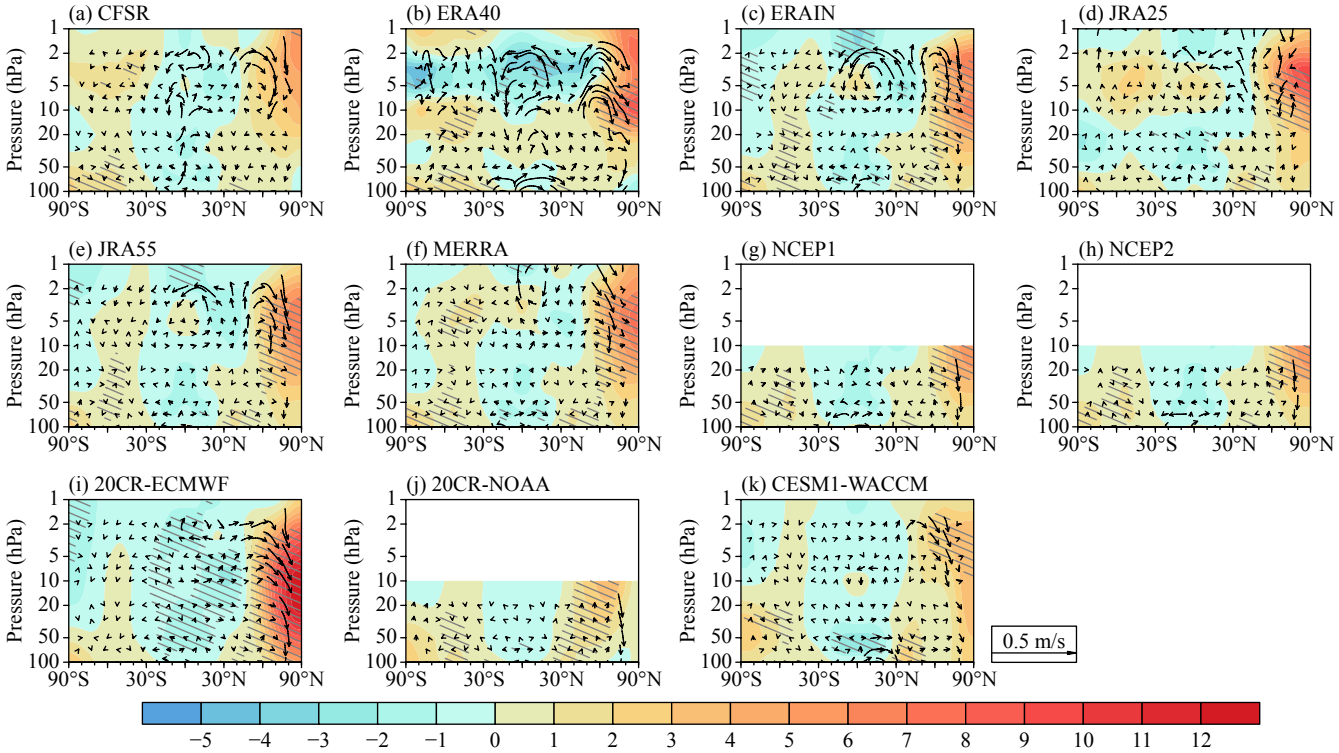

Figure 5. Composite differences in the zonal-mean temperature (shadings; units: K) and the scaled residual velocity ($\bar{v}^*$, $250\times\bar{w}^*$; vectors; units: m/s) between El Niño and La Niña winters from ten reanalyses and CESM1-WACCM, respectively. The hatched regions mark the temperature difference between El Niño and La Niña winters above the 90% confidence level.

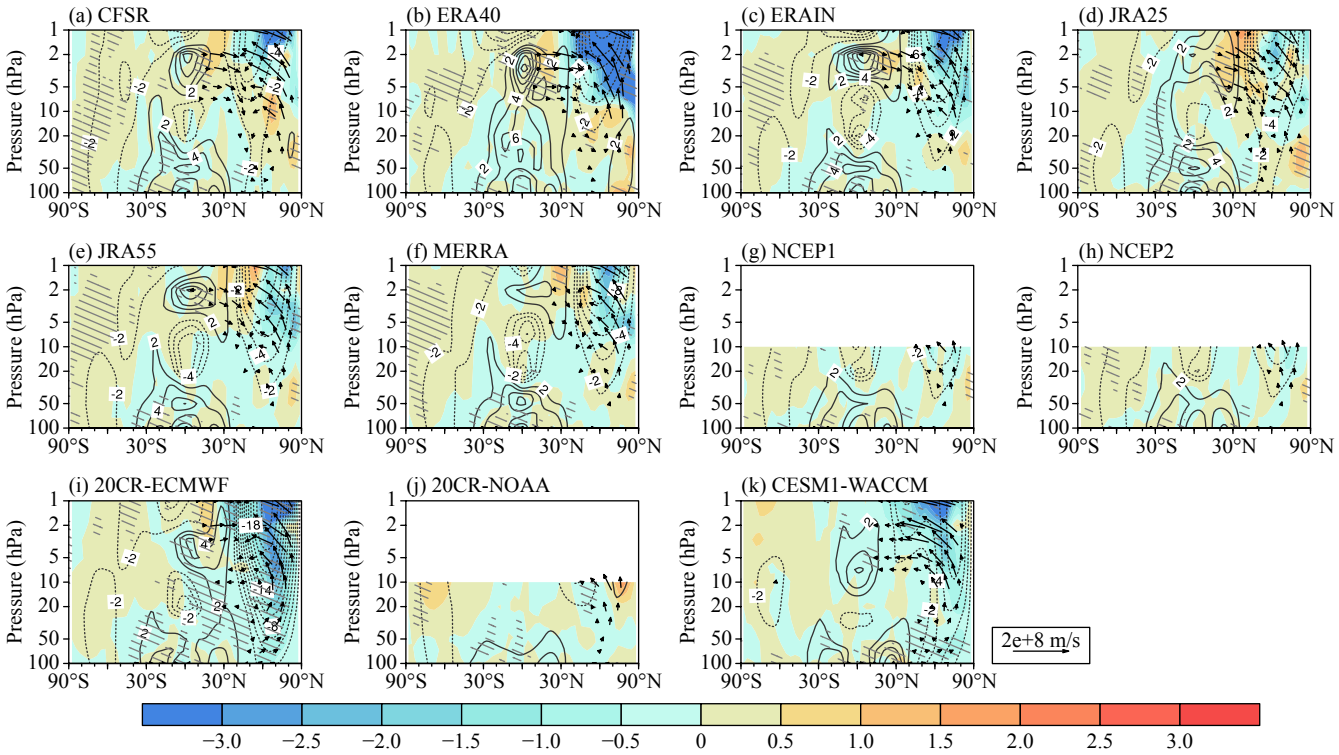

Figure 6. Composite differences in the zonal-mean zonal wind (contours; units: m/s), in the EP flux scaled by the local air density (F_y/ρ_0, $100\times F_z/\rho_0$; vectors; units: m^3/s^2), and EP flux divergence (shadings; units: m/s/d) between El Niño and La Niña winters from ten reanalyses and CESM1-WACCM, respectively. The hatched regions mark the EP flux divergence difference between El Niño and La Niña winters above the 90% confidence level.

and Ren RC, 2016a, b, c ; Lubis et al., 2018a). All of the ten reanalyses and CESM1-WACCM consistently reveal that the upward propagation of waves is enhanced in El Niño winters relative to La Niña winters. The strong negative EP flux divergence anomalies in the mid-to-high latitude stratosphere mean a strong dissipation of the planetary waves in the stratosphere, leading to strong easterly anomalies that are observed in all reanalyses and CESM1-WACCM. The maximum easterly response is 10 m/s in the upper stratosphere in most reanalyses, and the maximum easterly response is around 4 m/s at 10 hPa for NCEP1, NCEP2, and 20CR-NOAA. Consistent with the Arctic temperature response in 20CR-ECMWF, the EP divergence and circumpolar wind responses in 20CR-ECMWF are also the largest among reanalyses. Therefore, the stratospheric polar response to ENSO in 20CR-ECMWF is overestimated compared with other reanalyses, which is mainly caused by the over-strong wave dissipation in the mid-to-high latitudes, as well as an overestimated BDC response. The overestimated wave dissipation in 20CR-ECMWF is related to the mean flow biases in this reanalysis that can affect the transmission and refraction properties of vertically propagating planetary waves (e.g., Lubis et al., 2018b, c). The enhanced wave dissipation is also seen in CESM1-WACCM, which again verifies that the enhanced BDC response is associated with the intensified upward propagation of waves and their dissipation in the stratosphere in El Niño winters.

5.2 QBO

Figure 7 shows the composite differences in the residual velocity and the zonal-mean temperature between easterly and westerly QBO phase winters for the ten reanalyses and CESM1-WACCM, respectively. The easterly QBO usually corresponds to a negative Northern Annular Mode (NAM)-like response known as the Holton and Tan relationship (1980). The Holton and Tan relationship is consistently seen in most reanalyses (Figures 7a–h): Compared with westerly QBO phases, the stratospheric polar vortex is warmer and weaker in easterly QBO phases (White et al., 2015; Rao J and Ren RC, 2017, 2018). In contrast, 20CR-ECMWF fails to reproduce the Holton and Tan relationship, as shown in other eight reanalyses. Since the QBO is not resolved in 20CR-NOAA, it is expected that the modulation of the BDC by QBO is missing in this dataset. As the QBO forcing is turned on in CESM1-WACCM, the stratospheric polar vortex is also warm and weak in easterly QBO winters relative to westerly QBO winters.

Abalos et al. (2015) found that the variance of the tropical BDC upwelling explained by the QBO has a large spread among different estimates. Here we found that the BDC response to QBO seems to be much more consistent among different reanalyses based on the residual velocity than among different estimates in Abalos et al. (2015). In the tropical lower stratosphere, cold temperature anomalies appear below 50 hPa and warm temperature anomalies above 50 hPa by the thermal wind balance. To balance the temperature anomalies, upwelling is produced below 50 hPa and downwelling is produced from 50 to 10 hPa in the equator. To compensate the equatorial downwelling above the QBO zonal wind maximum level (50 hPa), an anomalous upwelling branch and cold temperature anomalies are excited in the midlatitude stratosphere. The secondary circulation cell (e.g., Baldwin et al.,

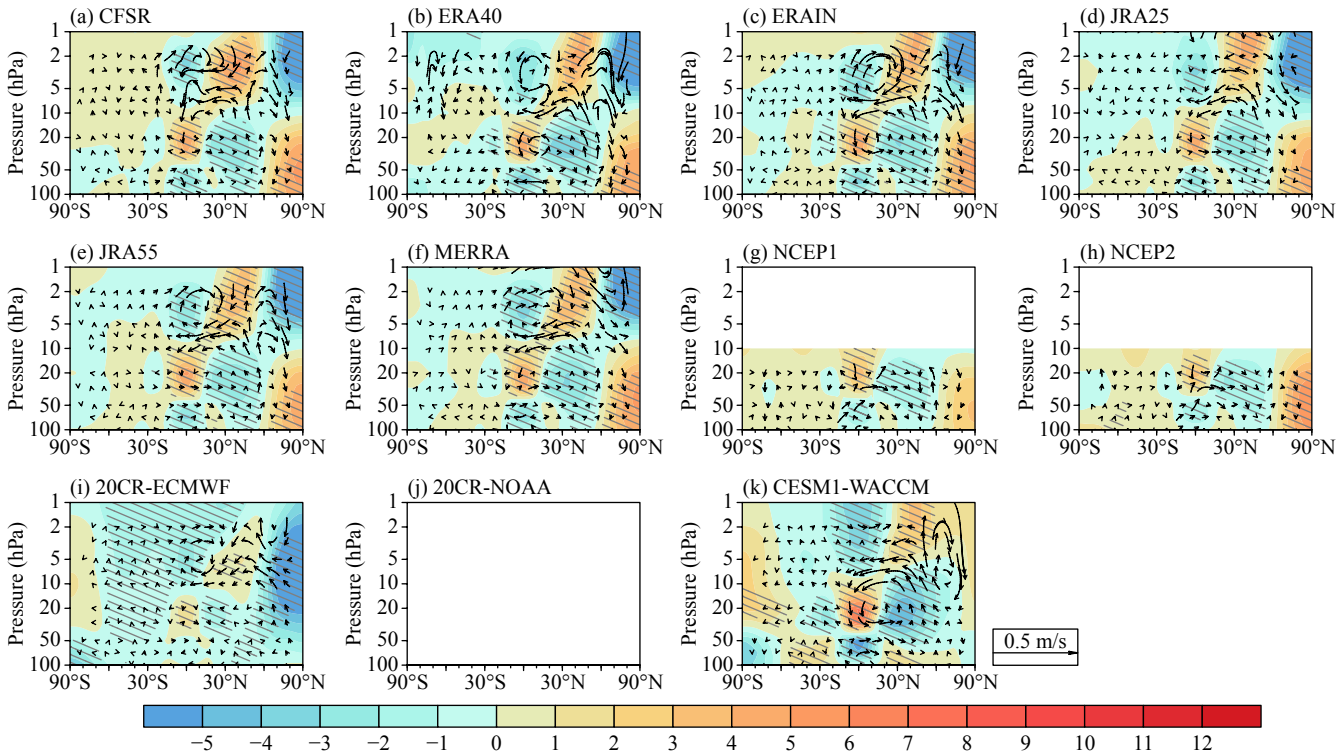

Figure 7. Composite differences in the zonal-mean temperature (shadings; units: K) and the scaled residual velocity ($\bar{v}^*$, $250\times\bar{w}^*$; vectors; units: m/s) between the easterly and westerly QBO winters from ten reanalyses and CESM1-WACCM, respectively. The hatched regions mark the temperature difference between the easterly and westerly QBO winters above the 90% confidence level.

2001) in the lowermost/middle stratosphere strengthens/weakens the shallow branch of the BDC in the tropics. Similarly, a secondary circulation cell is also seen above the 10 hPa in the equator, which is related to the cold anomalies in the equator and warm anomalies in midlatitudes above 10 hPa. The midlatitude downwelling in the upper stratosphere extends poleward and tilts downward, explaining the warm and weak polar vortex in the Arctic lower stratosphere. The secondary circulation cell response in the lowermost/middle stratosphere (shallow BDC) is much weaker in 20CR-ECMWF than in the first eight reanalyses, but the circulation cell in the upper stratosphere, as well as the cold anomalies in the equator and warm anomalies in midlatitudes above 10 hPa, is similar in those reanalyses. CESM1-WACCM successfully simulates the anticlockwise cell response in the middle stratosphere and the clockwise BDC in the upper stratosphere.

The composite differences in the zonal-mean zonal wind, the EP flux, and its divergence between easterly and westerly QBO winters from reanalyses and CESM1-WACCM are shown Figure 8. The wave sources are mainly located in the midlatitude stratosphere, characterized with poleward and upward propagation of waves and dissipation in the circumpolar stratosphere. The strong EP flux convergence in easterly QBO winters explains the strong easterly anomalies in the circumpolar stratosphere (Figures 8a–h), with the maximum easterly center at 10 hPa (10 m/s). Considering that the QBO zonal wind propagates downward in the equator, the zonal wind sign in the upper stratosphere is reversed relative to the zonal wind at 50 hPa. When the QBO easterly anomalies are maximized at 50 hPa, westerly anomalies are observed and centered above 10 hPa. No significant effect of QBO on the tropospheric wave forcing is seen in reanalyses (Garfinkel et al., 2012; White et al., 2015), and the vertical propagation of waves below 100 hPa is much weaker for the QBO composite than for the ENSO composite (compare Figures 6 and 8). In both the reanalyses and CESM1-WACCM the mechanism whereby the QBO influences the Arctic stratospheric vortex is internal to the stratosphere. The QBO mainly impacts the Arctic stratospheric vortex through the shift of the subtropical critical line in the lower stratosphere and through the change in mean meridional circulation in the upper stratosphere. The easterly anomalies in the equatorial lower stratosphere move the subtropical critical line further poleward in the lower stratosphere, and more waves propagate to the polar vortex and dissipate there (i.e., negative EP flux). The direct BDC response to QBO by the thermal wind balance changes the extratropical temperature anomalies (Figure 7) and creates a barrier (the positive EP flux divergence near 30°N) to wave propagation from the circumpolar region to midlatitudes in the upper stratosphere, also contributing to the weakening of the polar vortex.

Kim and Chun (2015) separated the momentum forcing of the QBO by equatorial waves in five reanalyses, and Kawatani et al. (2016) compared the representation of the QBO among major global atmospheric reanalysis datasets. To explore the differences between the two 20CRs and other reanalyses, we show the evolution of the equatorial zonal mean zonal wind from 100–1 hPa in Figure 9. The quasi biennial cycle of the equatorial zonal wind is

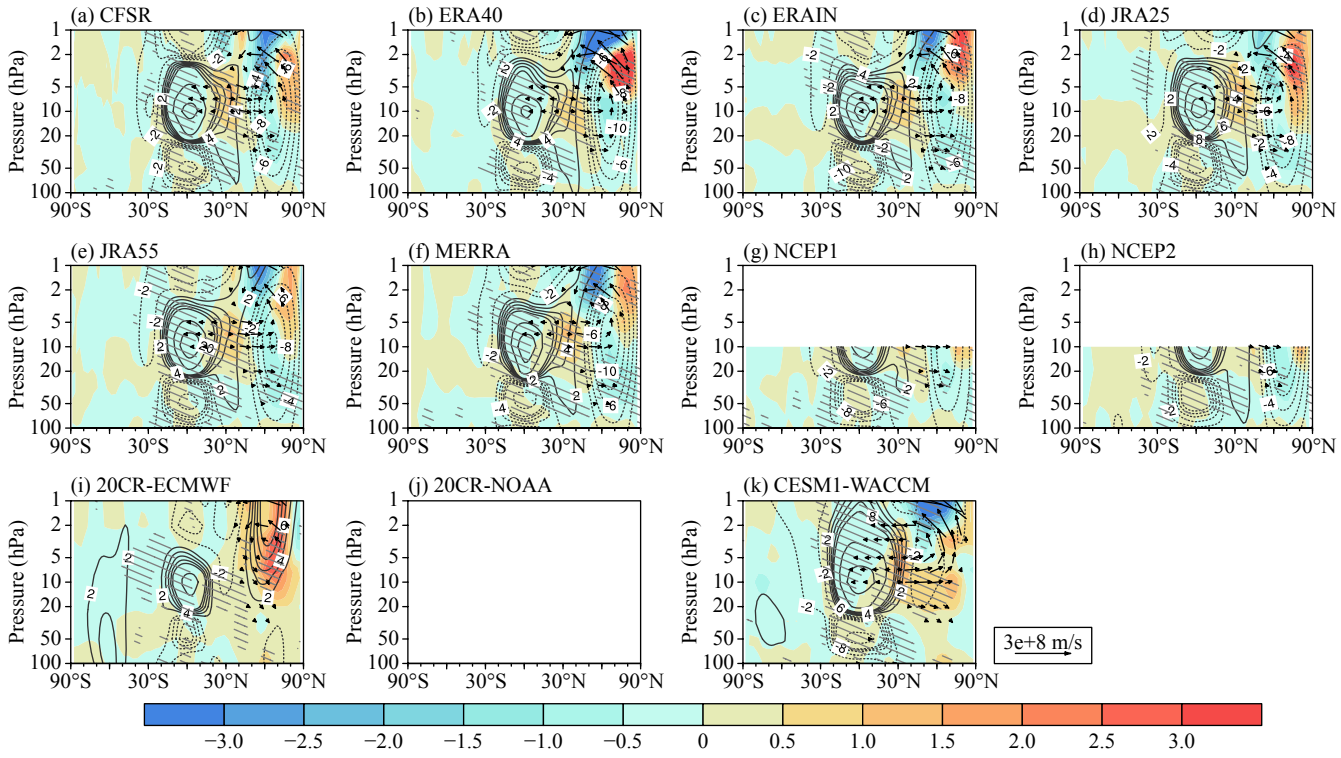

Figure 8. Composite differences in the zonal-mean zonal wind (contours; units: m/s), in the EP flux scaled by the local air density (F_y/ρ_0, $100\times F_z/\rho_0$; vectors; units: m³/s²), and EP flux divergence (shadings; units: m/s/d) between easterly and westerly QBO winters from ten reanalyses and CESM1-WACCM, respectively. The hatched regions mark the EP flux divergence difference between easterly and westerly QBO winters above the 90% confidence level.

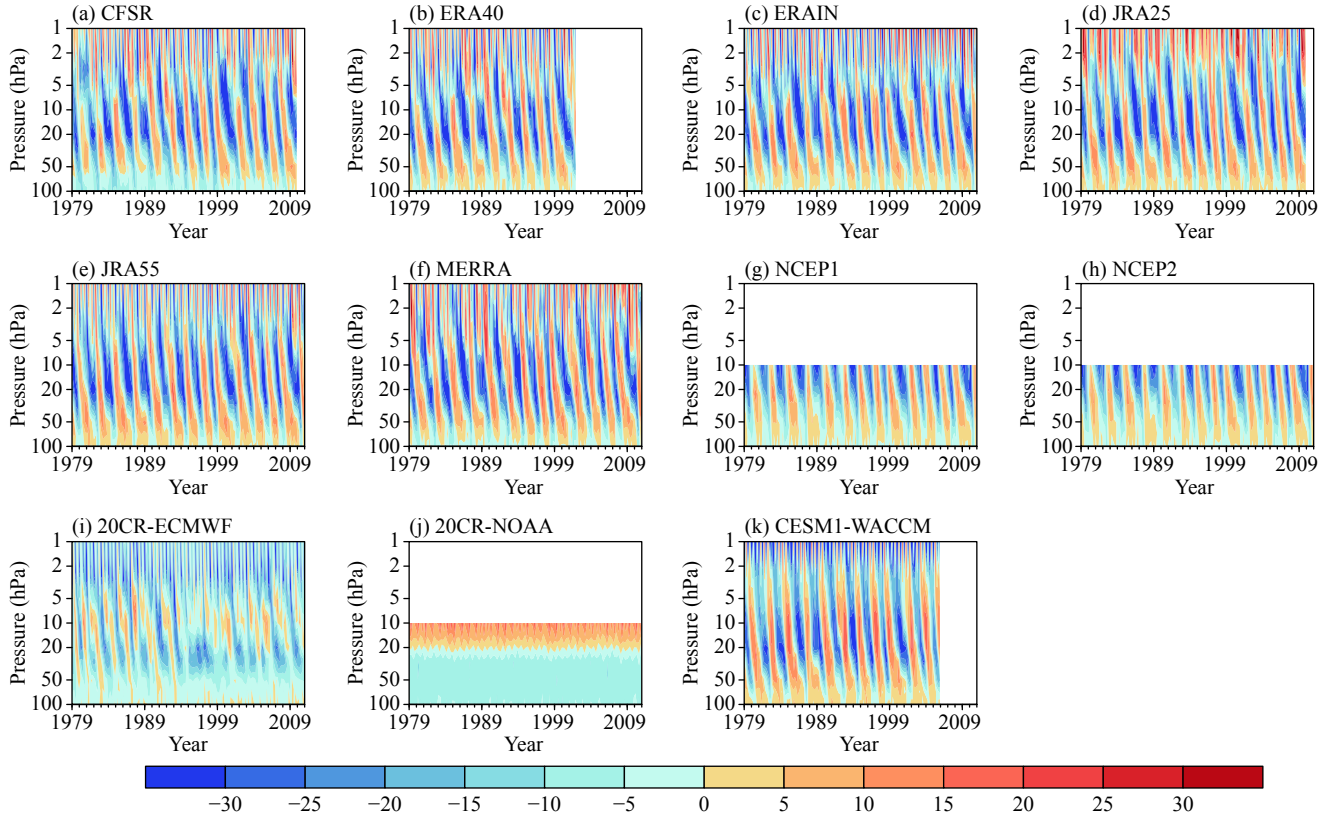

Figure 9. Pressure–time evolutions of the zonal-mean zonal wind (units: m/s) in the equator (5°S–5°N) from ten reanalyses and CESM1-WACCM, respectively.

resolved by most reanalyses except 20CR-ECMWF and 20CR-NOAA. The maximum westerly and easterly in 20CR-ECMWF is much weaker than in other reanalyses (10 vs 15, –20 vs –30 m/s), and the cycle of the equatorial zonal wind in 20CR-ECMWF is also shorter than in other reanalyses (Figure 9a–i). The QBO easterly period in the equatorial middle stratosphere is much longer than the QBO westerly period for 20CR-ECMWF, and the QBO westerly period is seldom identified in the equatorial lower stratosphere. In contrast, no QBO-like cycle is seen in 20CR-NOAA, and easterlies dominate in the lower troposphere. The QBO in the lower stratosphere and quasi semiannual oscillation in the upper stratosphere are seen in the first eight reanalyses and CESM1-WACCM, although the quasi semiannual oscillation transition timings are different between CESM1-WACCM and the reanalyses. It can be concluded that the lack of the Holton and Tan relationship in 20CR-ECMWF is caused by the disgraceful representation of QBO in the reanalysis system. Recent studies have identified the importance of radiative ozone waves for changes in the stratospheric temperature and the stratospheric polar vortex response to QBO by accumulating energy during fall and early winter and being amplified by wave-mean flow feedbacks in winter (e.g., Silverman et al., 2018). The reanalyses may be further improved if the ozone wave effects are considered in the reanalysis assimilation systems.

5.3 Solar Cycle

The composite differences in the residual velocity and the zonal-mean temperature between solar minimum and solar maximum winters are shown in Figure 10 for the ten reanalyses and CESM1-WACCM, respectively. The impact of the solar cycle on the stratospheric temperature and circulation has been noticed (Kodera and Kuroda, 2002; Camp and Tung, 2007; Rind et al., 2008). Although the Earth obtains less solar flux during solar minima than during solar maxima, a weakened stratospheric polar vortex is observed during solar minima (Rao J and Ren RC, 2017, 2018). Specifically, all the reanalyses and CESM1-WACCM show that the tropical and midlatitude stratosphere is anomalously cold during the solar minima. In the upper stratosphere, the deep branch of the BDC is weakened in the solar minima, which induces an upwelling over the Arctic associated with the cold center at 5 hPa (–5 K) and a downwelling in the subtropics where a patch of warm anomalies develops. In the lower stratosphere, the shallow branch of the BDC is intensified as shown in most reanalyses (Figures 10a–i), as well as in CESM1-WACCM (Figure 10k). The polar vortex is warmer and weaker in the lower stratosphere in response to the enhanced shallow branch of the BDC and the related downwelling over the Arctic. However, the 20CR-NOAA reanalysis fails to reproduce the warmer signal in the Arctic lower stratosphere, but the cold anomalies in the southern and tropical stratosphere are well simulated (Figure 10j).

Figure 11 shows the composite differences in the zonal-mean zonal wind and EP flux between solar minimum and solar maximum winters for reanalyses and CESM1-WACCM. The subtropical jet in the upper stratosphere is weakened in all reanalyses, which can be directly explained by the thermal wind balance (see the tem-

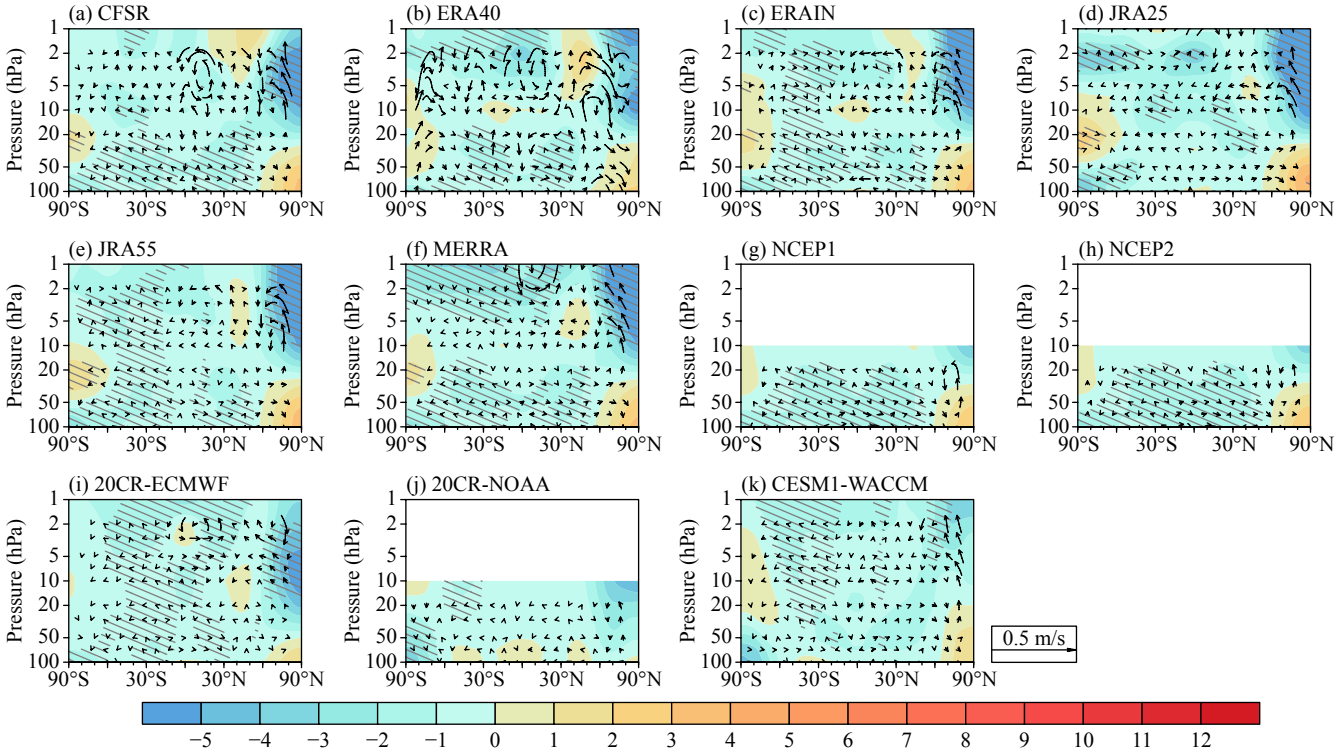

Figure 10. Composite differences in the zonal-mean temperature (shadings; units: K) and the scaled residual velocity ($\bar{v}^*$, $250\times\bar{w}^*$; vectors; units: m/s) between the solar minimum and solar maximum winters from ten reanalyses and CESM1-WACCM, respectively. The hatched regions mark the temperature difference between the solar minimum and solar maximum winters above the 90% confidence level.

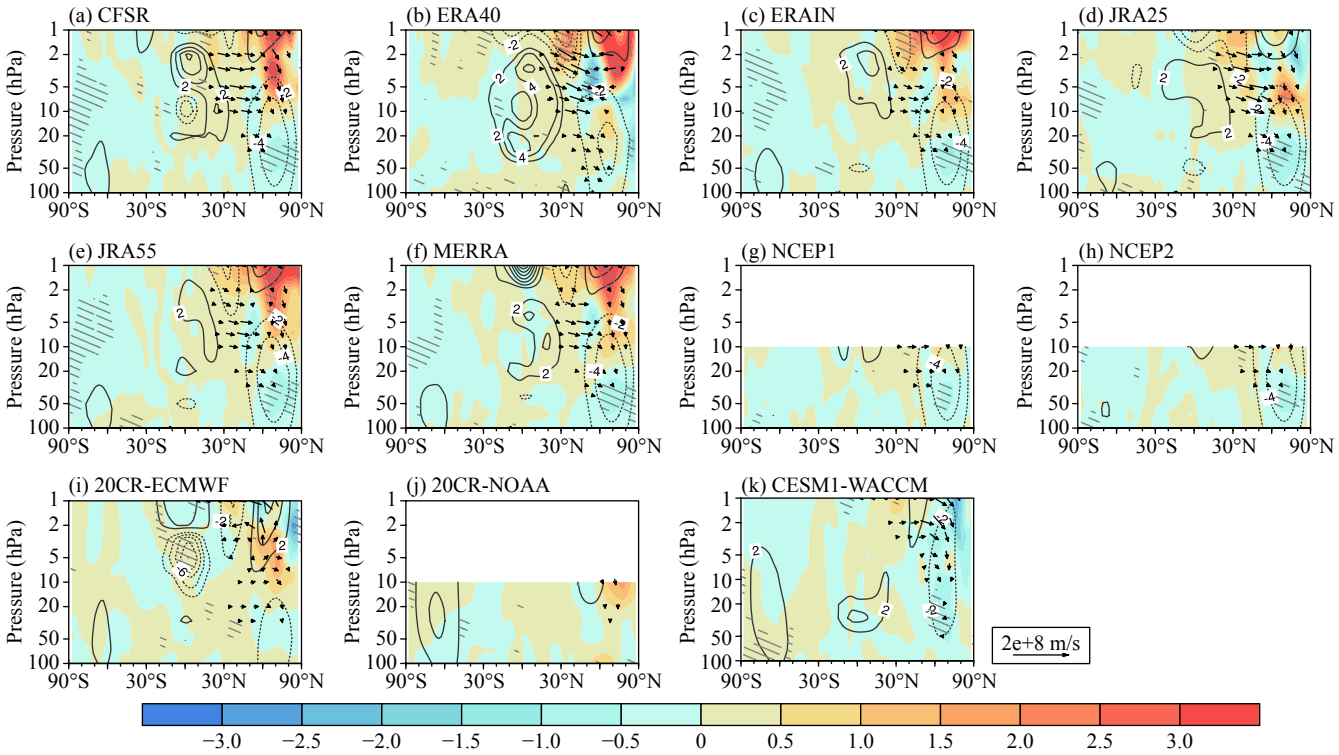

Figure 11. Composite differences in the zonal-mean zonal wind (contours; units: m/s), in the EP flux scaled by the local air density (F_y/ρ_0, $100\times F_z/\rho_0$; vectors; units: m³/s²), and EP flux divergence (shadings; units: m/s/d) between the solar minimum and solar maximum winters from ten reanalyses and CESM1-WACCM, respectively. The hatched regions mark the EP flux divergence difference between the solar minimum and solar maximum winters above the 90% confidence level.

perature anomaly distribution in Figure 10). The circumpolar westerly jet is weakened, associated with a negative NAM-like response during solar minima (Matthes et al., 2006), which is mainly attributed to the uneven distribution of the solar energy absorbed by the Earth and change in the background circulation. The midlatitude waves in the upper stratosphere propagate poleward and downward, dissipating in the Arctic lower stratosphere, leading to a deceleration of the circumpolar westerly jet (–4 m/s). Consistent with the strengthened BDC in the lower stratosphere, a negative NAM-like response can be found in the lower stratosphere during solar minima in most reanalyses (except 20CR-NOAA) and CESM1-WACCM: warm anomalies dominate over the Arctic and cold anomalies appear in the midlatitudes (Figure 10). Although the BDC response to the solar cycle is much weaker than that to ENSO and QBO (Rao J and Ren RC, 2017, 2018), the impacts of solar cycle on the polar cap temperature and circumpolar westerly jet in the lower stratosphere are robustly identified in reanalyses (2 K, –4 m/s) and CESM1-WACCM (1 K, –2 m/s).

6. Summary and Discussion

In this study, ten reanalyses and a stratosphere-resolving coupled model, CESM1-WACCM, are used to compare and assess the climatology and interannual variation of the northern winter stratospheric BDC estimated by the RMMSF. From the definition of residual velocity and the nondivergent form of the continuity equation in spherical coordinates, the RMMSF is derived by vertically integrating the residual meridional velocity. The northern winter BDC is a large-scale well-organized meridional circulation in the stratosphere. The winter hemispheric BDC is much stronger and deeper than the summer hemispheric counterpart. The general pattern of the northern winter BDC is quite consistent among reanalyses, but the tropical upward mass flux associated with the BDC varies with the dataset. The tropical upward mass flux is underestimated in CFSR, 20CR-ECMWF, and 20CR-NOAA when compared with other datasets. On the contrary, the tropical upwelling is overestimated in ERA40, JRA25, and NCEP1 when compared with the reanalysis ensemble mean and CESM1-WACCM. The tropical vertical mass flux at 100 hPa shows a large inter-reanalysis spread, but this difference decreases at 70 hPa.

The interannual variation and long-term trend of the tropical upward mass flux at 100 hPa and 70 hPa are also compared and assessed among reanalyses. The time trend of the BDC upwelling during 1979–2010 largely depends on the reanalysis used. The decreasing trend of the BDC identified from ERAIN in previous studies (Iwasaki et al., 2009; Abalos et al., 2015; Wang WG et al., 2015) is confirmed. The linear trend for the tropical upward mass flux is contrastingly different in other reanalyses. Most reanalyses show an accelerating trend for the tropical upward mass flux during 1979–2010. The linear trend of the tropical upward mass flux is also positive at 100 hPa and 70 hPa in the CESM1-WACCM historical run forced by natural and anthropogenic forcings, consistent with most reanalyses.

Changes in BDC may be a bridge linking stratospheric circulation anomalies with ENSO, QBO, and solar cycle. All reanalyses and CESM1-WACCM reveal that the BDC is enhanced in El Niño winters compared with La Niña winters. The upward propagation of waves from the troposphere to the stratosphere is strengthened in the extratropics, and the meridional propagation of waves in the stratosphere is of secondary importance for the polar vortex response to ENSO. As the wave forcing becomes stronger in El Niño winters, the deep and shallow branches of the BDC are intensified. The enhanced BDC well explains the weak and warm stratosphere polar vortex observed in El Niño winters due to the adiabatic heating caused by the enhanced BDC downwelling in the extratropics. The BDC response to QBO agrees with the Holton and Tan relationship in most reanalyses in the lowermost stratosphere: the shallow branch of the BDC is strengthened by the upwelling below the QBO easterly center at 50 hPa to balance the cold anomalies in the equator and the downwelling in midlatitudes, moving the subtropical critical line further poleward in the lower stratosphere. The direct BDC response to QBO in the upper stratosphere creates a barrier near 30°N to prevent waves from propagating to midlatitudes, also contributing to the weakening of the polar vortex. The quasi biennial cycle of the stratospheric equatorial zonal wind is shorter in 20CR-ECMWF than that in other reanalyses, and the oscillation intensity is also underestimated. The BDC response to QBO in 20CR-ECMWF is much weaker than in other reanalyses and CESM1-WACCM. The QBO is not resolved in 20CR-NOAA, and the Holton and Tan relationship is also missing. The BDC response to solar cycle is relatively weak in all datasets when compared with its response to ENSO and QBO, implying the importance of thermodynamics in distribution of the solar flux. The shallow branch of the BDC in the lower stratosphere is intensified during solar minima in most reanalyses and in CESM1-WACCM. In response to the enhanced shallow branch of the BDC, the polar vortex in the Arctic lower stratosphere is warmer and weaker. The midlatitude waves in the upper stratosphere propagate poleward and downward, dissipating in the Arctic lower stratosphere, also contributing to the weakening of the stratospheric polar vortex.

Previous studies have identified a decelerating BDC in recent decades as the global mean temperature has risen (Wang WG et al., 2013, 2015) from ERAIN. Our results confirm the long-term decrease in the tropical upward mass flux from stratosphere to troposphere during 1979–2010 in ERAIN. However, we find that this conclusion is rather sensitive to the choice of reanalyses, suggesting that more investments in these products are still required to obtain a unified map for the BDC trend and the mechanisms whereby the changes are forced (Miyazaki et al., 2016). As in previous model studies (Butchart et al., 2006, 2010; Garcia and Randel, 2008; Oberländer-Hayn et al., 2016; Lubis et al., 2018a), most reanalyses also show that the tropical upwelling of the BDC increases. The discrepancies in the winter BDC between reanalyses might also be related to different parameterized eddy mixing schemes, as well as different strengths of total wave damping in the reanalysis assimilation systems (Lubis et al., 2018b, c ; Orsolini et al., 2018). Despite the satellite era data compared in this study, much uncertainty still exists among different reanalyses. A comprehensive comparison of the BDC in state-of-the-art climate models is still lacking, and thus worth further exploration in future studies.

Acknowledgments

We would like to thank the editor T. J. Zhou and two anonymous reviewers, whose comments improve the presentation of the paper. This work was jointly supported by grants from the National Natural Science Foundation of China (41705024, 41875048), the National Key R&D Program of China (2016YFA0602104), the Planning and Budgeting Committee of the Council for Higher Education in Israel, and the Startup Foundation for Introducing Talent of NUIST (2016r060). We acknowledge the NOAA, NCEP, ECMWF, JMA, and NASA for providing the multiple reanalyses.

References

Abalos, M., Legras, B., Ploeger, F., and Randel, W. J. (2015). Evaluating the advective Brewer-Dobson circulation in three reanalyses for the period 1979–2012. *J. Geophys. Res. Atmos.*, *120*(15), 7534–7554. https://doi.org/10.1002/2015JD023182

Andrews, D. G., Holton, J. R., and Leovy, C. B. (1987). *Middle Atmosphere Dynamics* (pp. 489). San Diego: Academic Press.

Baldwin, M. P., Gray, L. J., Dunkerton, T. J., Hamilton, K., Haynes, P. H., Randel, W. J., Holton, J. R., Alexander, M. J., Hirota, I., … Takahashi, M. (2001). The Quasi-Biennial oscillation. *Rev. Geophys.*, *39*(2), 179–229. https://doi.org/10.1029/1999RG000073

Baldwin, M. P., Thompson, D. W. J., Shuckburgh, E. F., Norton, W. A., and Gillett, N. P. (2003). Weather from the stratosphere?. *Science*, *301*(5631), 317–319. https://doi.org/10.1126/science.1085688

Birner, T., and Bönisch, H. (2011). Residual circulation trajectories and transit times into the extratropical lowermost stratosphere. *Atmos. Chem. Phys.*, *11*(2), 817–827. https://doi.org/10.5194/acp-11-817-2011

Brewer, A. W. (1949). Evidence for a world circulation provided by the measurements of helium and water vapour distribution in the stratosphere. *Quart. J. Roy. Meteor. Soc.*, *75*(326), 351–363. https://doi.org/10.1002/qj.49707532603

Butchart, N., Scaife, A. A., Bourqui, M., de Grandpré, J., Hare, S. H. E., Kettleborough, J., Langematz, U., Manzini, E., Sassi, F., … Sigmond, M. (2006). Simulations of anthropogenic change in the strength of the Brewer-Dobson circulation. *Climate Dyn.*, *27*(7–8), 727–741. https://doi.org/10.1007/s00382-006-0162-4

Butchart, N., Cionni, I., Eyring, V., Shepherd, T. G., Waugh, D. W., Akiyoshi, H., Austin, J., Brühl, C., Chipperfield, M. P., … Tian, W. (2010). Chemistry-Climate Model simulations of twenty-first century stratospheric climate and circulation changes. *J. Climate*, *23*(20), 5349–5374. https://doi.org/10.1175/2010JCLI3404.1

Butchart, N. (2014). The Brewer-Dobson circulation. *Rev. Geophys.*, *52*(2), 157–184. https://doi.org/10.1002/2013RG000448

Calvo, N., Garcia, R. R., Randel, W. J., and Marsh, D. R. (2010). Dynamical mechanism for the increase in tropical upwelling in the lowermost tropical stratosphere during warm ENSO events. *J. Atmos. Sci.*, *67*(7), 2331–2340. https://doi.org/10.1175/2010JAS3433.1

Camp, C. D., and Tung, K. K. (2007). The influence of the solar cycle and QBO on the late-winter stratospheric polar vortex. *J. Atmos. Sci.*, *64*(4), 1267–1283. https://doi.org/10.1175/Jas3883.1

Compo, G. P., Whitaker, J. S., Sardeshmukh, P. D., Matsui, N., Allan, R. J., Yin, X., Gleasonm, B. E., Vose, R. S., Rutledge, G., … Worley, S. J. (2011). The Twentieth century reanalysis project. *Quart. J. Roy. Meteor. Soc.*, *137*(654), 1–28. https://doi.org/10.1002/qj.776

de la Cámara, A., Abalos, M., Hitchcock, P., Calvo, N., and Garcia, R. R. (2018). Response of Arctic ozone to sudden stratospheric warmings. *Atmos. Chem. Phys.*, *18*(22), 16499–16513. https://doi.org/10.5194/acp-18-16499-2018

Dee, D. P., Uppala, S. M., Simmons, A. J., Berrisford, P., Poli, P., Kobayashi, S., Andrae, U., Balmaseda, M. A., Balsamo, G., … Vitart, F. (2011). The ERA-Interim reanalysis: configuration and performance of the data assimilation system. *Quart. J. Roy. Meteor. Soc.*, *137*(656), 553–597. https://doi.org/10.1002/qj.828

Dobson, G. M. B., and Massey, H. S. W. (1956). Origin and distribution of the polyatomic molecules in the atmosphere. *Proc. Roy. Soc. London A Math. Phys. Sci.*, *236*(1205), 187–193. https://doi.org/10.1098/rspa.1956.0127

Ebita, A., Kobayashi, S., Ota, Y., Moriya, M., Kumabe, R., Onogi, K., Harada, Y., Yasui, S., Miyaoka, K., … Ishimizu, T. (2011). The Japanese 55-year Reanalysis "JRA-55": An Interim Report. *SOLA*, *7*, 149–152. https://doi.org/10.2151/sola.2011-038

Engel, A., Möbius, T., Bönisch, H., Schmidt, U., Heinz, R., Levin, I., Atlas, E., Aoki, S., Nakazawa, T., … Boering, K. (2008). Age of stratospheric air unchanged within uncertainties over the past 30 years. *Nat. Geosci.*, *2*, 28–31. https://doi.org/10.1038/ngeo388

Forster, P. M. D. F., and Shine, K. P. (1999). Stratospheric water vapour changes as a possible contributor to observed stratospheric cooling. *Geophys. Res. Lett.*, *26*(21), 3309–3312. https://doi.org/10.1029/1999gl010487

Fujiwara, M., Wright, J. S., Manney, G. L., Gray, L. J., Anstey, J., Birner, T., Davis, S., Gerber, E. P., Harvey, V. L., … Wargan, K. (2017). Introduction to the SPARC Reanalysis Intercomparison Project (S-RIP) and overview of the reanalysis systems. *Atmos. Chem. Phys.*, *17*(2), 1417–1452. https://doi.org/10.5194/acp-17-1417-2017

Garcia, R. R., and Randel, W. J. (2008). Acceleration of the Brewer–Dobson circulation due to increases in greenhouse gases. *J. Atmos. Sci.*, *65*(8), 2731–2739. https://doi.org/10.1175/2008jas2712.1

Garfinkel, C. I., and Hartmann, D. L. (2008). Different ENSO teleconnections and their effects on the stratospheric polar vortex?. *J. Geophys. Res.*, *113*(D18), D18114. https://doi.org/10.1029/2008jd009920

Garfinkel, C. I., Shaw, T. A., Hartmann, D. L., and Waugh, D. W. (2012). Does the Holton-Tan mechanism explain how the Quasi-Biennial Oscillation modulates the Arctic Polar vortex. *J. Atmos. Sci.*, *69*(5), 1713–1733. https://doi.org/10.1175/JAS-D-11-0209.1

Gray, L. J., Crooks, S., Pascoe, C., Sparrow, S., and Palmer, M. (2004). Solar and QBO influences on the timing of stratospheric sudden warmings. *J. Atmos. Sci.*, *61*(23), 2777–2796. https://doi.org/10.1175/JAS-3297.1

Haynes, P. H., McIntyre, M. E., Shepherd, T. G., Marks, C. J., and Shine, K. P. (1991). On the "downward control" of extratropical diabatic circulations by eddy-induced mean zonal forces. *J. Atmos. Sci.*, *48*(4), 651–678. https://doi.org/10.1175/1520-0469(1991)048<0651:OTCOED>2.0.CO;2

Hersbach, H., Peubey, C., Simmons, A., Berrisford, P., Poli, P., and Dee, D. (2015). ERA-20CM: a twentieth-century atmospheric model ensemble. *Quart. J. Meteor. Roy. Soc.*, *141*(691), 2350–2375. https://doi.org/10.1002/qj.2528

Holton, J. R., and Tan, H. C. (1980). The influence of the equatorial quasi-biennial oscillation on the global circulation at 50 mb. *J. Atmos. Sci.*, *37*(10), 2200–2208. https://doi.org/10.1175/1520-0469(1980)037<2200:TIOTEQ>2.0.CO;2

Holton, J. R. (1990). On the global exchange of mass between the stratosphere and troposphere. *J. Atmos. Sci.*, *47*(3), 392–395. https://doi.org/10.1175/1520-0469(1990)047<0392:OTGEOM>2.0.CO;2

Hu, J. G., Li, T., Xu, H. M., and Yang, S. Y. (2017). Lessened response of boreal winter stratospheric polar vortex to El Niño in recent decades. *Climate Dyn.*, *49*(1–2), 263–278. https://doi.org/10.1007/s00382-016-3340-z

Hu, Y. Y., and Tung, K. K. (2002). Interannual and decadal variations of planetary wave activity, stratospheric cooling, and Northern Hemisphere Annular mode. *J. Climate*, *15*(13), 1659–1673. https://doi.org/10.1175/1520-0442(2002)015<1659:IADVOP>2.0.CO;2

Iwasaki, T., Hamada, H., and Miyazaki, K. (2009). Comparisons of Brewer-Dobson circulations diagnosed from reanalyses. *J. Meteor. Soc. Japan*, *87*(6), 997–1006. https://doi.org/10.2151/jmsj.87.997

Kalnay, E., Kanamitsu, M., Kistler, R., Collins, W., Deaven, D., Gandin, L., Iredell, M., Saha, S., White, G., … Joseph, D. (1996). The NCEP/NCAR 40-year reanalysis project. *Bull. Amer. Meteor. Soc.*, *77*(3), 437–472. https://doi.org/10.1175/1520-0477(1996)077<0437:TNYRP>2.0.CO;2

Kanamitsu, M., Ebisuzaki, W., Woollen, J., Yang, S. K., Hnilo, J. J., Fiorino, M., and Potter, G. L. (2002). NCEP-DOE AMIP-Ⅱ Reanalysis (R-2). *Bull. Amer. Meteor. Soc.*, *83*(11), 1631–1643. https://doi.org/10.1175/bams-83-11-1631

Kawatani, Y., Hamilton, K., Miyazaki, K., Fujiwara, M., and Anstey, J. A. (2016). Representation of the tropical stratospheric zonal wind in global atmospheric reanalyses. *Atmos. Chem. Phys.*, *16*(11), 6681–6699.

https://doi.org/10.5194/acp-16-6681-2016

Kim, Y. H., and Chun, H. Y. (2015). Momentum forcing of the Quasi-Biennial Oscillation by equatorial waves in recent reanalyses. *Atmos. Chem. Phys.*, *15*(12), 6577–6587. https://doi.org/10.5194/acp-15-6577-2015

Kodera, K., and Kuroda, Y. (2002). Dynamical response to the solar cycle. *J. Geophys. Res.*, *107*(D24), ACL 5-1–ACL 5-12. https://doi.org/10.1029/2002JD002224

Lossow, S., McLandress, C., Jonsson, A. I., and Shepherd, T. G. (2012). Influence of the Antarctic ozone hole on the polar mesopause region as simulated by the Canadian Middle Atmosphere Model. *J. Atmos. Sol. Terr. Phys.*, *74*, 111–123. https://doi.org/10.1016/j.jastp.2011.10.010

Lubis, S. W., Omrani, N. E., Matthes, K., and Wahl, S. (2016). Impact of the Antarctic ozone hole on the vertical coupling of the stratosphere–mesosphere–lower thermosphere system. *J. Atmos. Sci.*, *73*(6), 2509–2528. https://doi.org/10.1175/JAS-D-15-0189.1

Lubis, S. W., Silverman, V., Matthes, K., Harnik, N., Omrani, N. E., and Wahl, S. (2017). How does downward planetary wave coupling affect polar stratospheric ozone in the Arctic winter stratosphere?. *Atmos. Chem. Phys.*, *17*(3), 2437–2458. https://doi.org/10.5194/acp-17-2437-2017

Lubis, S. W., Matthes, K., Harnik, N., Omrani, N. E., and Wahl, S. (2018a). Downward wave coupling between the stratosphere and troposphere under future anthropogenic climate change. *J. Climate*, *31*(10), 4135–4155. https://doi.org/10.1175/JCLI-D-17-0382.1

Lubis, S. W., Huang, C. S. Y., and Nakamura, N. (2018b). Role of finite-amplitude eddies and mixing in the life cycle of stratospheric sudden warmings. *J. Atmos. Sci.*, *75*(11), 3987–4003. https://doi.org/10.1175/JAS-D-18-0138.1

Lubis, S. W., Huang, C. S. Y., Nakamura, N., Omrani, N. E., and Jucker, M. (2018c). Role of finite-amplitude Rossby waves and nonconservative processes in downward migration of extratropical flow anomalies. *J. Atmos. Sci.*, *75*(5), 1385–1401. https://doi.org/10.1175/JAS-D-17-0376.1

Marsh, D. R., Mills, M. J., Kinnison, D. E., Lamarque, J. F., Calvo, N., and Polvani, L. M. (2013). Climate change from 1850 to 2005 simulated in CESM1 (WACCM). *J. Climate*, *26*(19), 7372–7391. https://doi.org/10.1175/JCLI-D-12-00558.1

Matthes, K., Kuroda, Y., Kodera, K., and Langematz, U. (2006). Transfer of the solar signal from the stratosphere to the troposphere: Northern winter. *J. Geophys. Res.*, *111*(D6), D06108. https://doi.org/10.1029/2005jd006283

McLandress, C., and Shepherd, T. G. (2009). Simulated anthropogenic changes in the Brewer–Dobson circulation, including its extension to high latitudes. *J. Climate*, *22*(6), 1516–1540. https://doi.org/10.1175/2008jcli2679.1

Miyazaki, K., Iwasaki, T., Kawatani, Y., Kobayashi, C., Sugawara, S., and Hegglin, M. I. (2016). Inter-comparison of stratospheric mean-meridional circulation and eddy mixing among six reanalysis data sets. *Atmos. Chem. Phys.*, *16*(10), 6131–6152. https://doi.org/10.5194/acp-16-6131-2016

Oberländer-Hayn, S., Gerber, E. P., Abalichin, J., Akiyoshi, H., Kerschbaumer, A., Kubin, A., Kunze, M., Langematz, U., Meul, S., … Oman, L. D. (2016). Is the Brewer-Dobson circulation increasing or moving upward?. *Geophys. Res. Lett.*, *43*(4), 1772–1779. https://doi.org/10.1002/2015GL067545

Onogi, K., Tsutsui, J., Koide, H., Sakamoto, M., Kobayashi, S., Hatsushika, H., Matsumoto, T., Yamazaki, N., Kamahori, H., … Taira, R. (2007). The JRA-25 reanalysis. *J. Meteor. Soc. Japan*, *85*(3), 369–432. https://doi.org/10.2151/jmsj.85.369

Orsolini, Y. J., Nishii, K., and Nakamura, H. (2018). Duration and decay of Arctic stratospheric vortex events in the ECMWF seasonal forecast model. *Quart. J. Roy. Meteor. Soc.*, *144*(717), 2876–2888. https://doi.org/10.1002/qj.3417

Plumb, R. A. (2002). Stratospheric transport. *J. Meteor. Soc. Japan*, *80*(4B), 793–809. https://doi.org/10.2151/jmsj.80.793

Polvani, L. M., and Kushner, P. J. (2002). Tropospheric response to stratospheric perturbations in a relatively simple general circulation model. *Geophys. Res. Lett.*, *29*(7), 18-1–18-4. https://doi.org/10.1029/2001gl014284

Polvani, L. M., Abalos, M., Garcia, R., Kinnison, D., and Randel, W. J. (2018). Significant weakening of Brewer-Dobson circulation trends over the 21st century as a consequence of the Montreal Protocol. *Geophys. Res. Lett.*, *45*(1), 401–409. https://doi.org/10.1002/2017GL075345

Randel, W. J., Garcia, R. R., Calvo, N., and Marsh, D. (2009). ENSO influence on zonal mean temperature and ozone in the tropical lower stratosphere. *Geophys. Res. Lett.*, *36*(15), L15822. https://doi.org/10.1029/2009gl039343

Rao, J., Ren, R. C. and Yang, Y. (2015). Parallel comparison of the northern winter stratospheric circulation in reanalysis and in CMIP5 models. *Adv. Atmos. Sci.*, *32*(7), 952–966. https://doi.org/10.1007/s00376-014-4192-2

Rao, J., and Ren, R. C. (2016a). A decomposition of ENSO's impacts on the northern winter stratosphere: Competing effect of SST forcing in the tropical Indian Ocean. *Climate Dyn.*, *46*(11–12), 3689–3707. https://doi.org/10.1007/s00382-015-2797-5

Rao, J., and Ren, R. C. (2016b). Asymmetry and nonlinearity of the influence of ENSO on the northern winter stratosphere: 1. Observations. *J. Geophys. Res. Atmos.*, *121*(15), 9000–9016. https://doi.org/10.1002/2015jd024520

Rao, J., and Ren, R. C. (2016c). Asymmetry and nonlinearity of the influence of ENSO on the northern winter stratosphere: 2. Model study with WACCM. *J. Geophys. Res. Atmos.*, *121*(15), 9017–9032. https://doi.org/10.1002/2015jd024521

Rao, J., and Ren, R. C. (2017). Parallel comparison of the 1982/83, 1997/98 and 2015/16 super El Niños and their effects on the extratropical stratosphere. *Adv. Atmos. Sci.*, *34*(9), 1121–1133. https://doi.org/10.1007/s00376-017-6260-x

Rao, J., and Ren, R. C. (2018). Varying stratospheric responses to tropical Atlantic SST forcing from early to late winter. *Climate Dyn.*, *51*(5–6), 2079–2096. https://doi.org/10.1007/s00382-017-3998-x

Rayner, N. A., Parker, D. E., Horton, E. B., Folland, C. K., Alexander, L. V., Rowell, D. P., Kent, E. C., and Kaplan, A. (2003). Global analyses of sea surface temperature, sea ice, and night marine air temperature since the late nineteenth century. *J. Geophys. Res. Atmos.*, *108*(D14), 4407. https://doi.org/10.1029/2002jd002670

Ren, R. C., Rao, J., Wu, G. X., and Cai, M. (2017). Tracking the delayed response of the northern winter stratosphere to ENSO using multi reanalyses and model simulations. *Climate Dyn.*, *48*(9–10), 2859–2879. https://doi.org/10.1007/s00382-016-3238-9

Rienecker, M. M., Suarez, M. J., Gelaro, R., Todling, R., Bacmeister, J., Liu, E., Bosilovich, M. G., Schubert, S. D., Takacs, L., … Woollen, J. (2011). MERRA: NASA's modern-era retrospective analysis for research and applications. *J. Climate*, *24*(14), 3624–3648. https://doi.org/10.1175/jcli-d-11-00015.1

Rind, D., Suozzo, R., Balachandran, N. K., and Prather, M. J. (1990). Climate change and the middle atmosphere. Part Ⅰ: The doubled CO_2 climate. *J. Atmos. Sci.*, *47*(4), 475–494. https://doi.org/10.1175/1520-0469(1990)047<0475:CCATMA>2.0.CO;2

Rind, D., Lean, J., Lerner, J., Lonergan, P., and Leboissitier, A. (2008). Exploring the stratospheric/tropospheric response to solar forcing. *J. Geophys. Res. Atmos.*, *113*(D24), D24103. https://doi.org/10.1029/2008jd010114

Roscoe, H. K. (2006). The Brewer–Dobson circulation in the stratosphere and mesosphere–Is there a trend?. *Adv. Space Res.*, *38*(11), 2446–2451. https://doi.org/10.1016/j.asr.2006.02.078

Rosenlof, K. H., and Holton, J. R. (1993). Estimates of the stratospheric residual circulation using the downward control principle. *J. Geophys. Res. Atmos.*, *98*(D6), 10465–10479. https://doi.org/10.1029/93JD00392

Rosenlof, K. H. (1995). Seasonal cycle of the residual mean meridional circulation in the stratosphere. *J. Geophys. Res. Atmos.*, *100*(D3), 5173–5191. https://doi.org/10.1029/94JD03122

Saha, S., Moorthi, S., Pan, H. L., Wu, X. R., Wang, J. D., Nadiga, S., Tripp, P., Kistler, R., Woollen, J., … Goldberg, M. (2010). The NCEP climate forecast system reanalysis. *Bull. Amer. Meteor. Soc.*, *91*(8), 1015–1058. https://doi.org/10.1175/2010bams3001.1

Seviour, W. J. M., Butchart, N., and Hardiman, S. C. (2012). The Brewer-Dobson circulation inferred from ERA-Interim. *Quart. J. Roy. Meteor. Soc.*, *138*(665), 878–888. https://doi.org/10.1002/qj.966

Shepherd, T. G. (2007). Transport in the middle atmosphere. *J. Meteor. Soc. Japan*, *85B*, 165–191. https://doi.org/10.2151/jmsj.85b.165

Silverman, V., Harnik, N., Matthes, K., Lubis, S. W., and Wahl, S. (2018). Radiative effects of ozone waves on the Northern Hemisphere polar vortex and its modulation by the QBO. *Atmos. Chem. Phys.*, *18*(9), 6637–6659. https://doi.org/10.5194/acp-18-6637-2018

Simpson, I. R., Shepherd, T. G., and Sigmond, M. (2011). Dynamics of the lower

stratospheric circulation response to ENSO. *J. Atmos. Sci.*, *68*(11), 2537–2556. https://doi.org/10.1175/JAS-D-11-05.1

Uppala, S. M., KÅllberg, P. W., Simmons, A. J., Andrae, U., Bechtold, V. D. C., Fiorino, M., Gibson, J. K., Haseler, J., Hernandez, A., … Woollen, J. (2005). The ERA-40 re-analysis. *Quart. J. Roy. Meteor. Soc.*, *131*(612), 2961–3012. https://doi.org/10.1256/qj.04.176

Wang, W. G., Yang, F. Y., Zheng, J. M., Wang, H. Y., Fan, W. X., Yu, K., Chai, S. Y., and Hu, T. (2013). A study on the trend of the Brewer-Dobson circulation in light of the downward control principle. *J. Yunnan Univ.* , *35*(3), 328–337. https://doi.org/10.7540/j.ynu.20130099

Wang, W. G., Yang, F. Y., Wang, H. Y., Yang, T., Yu, K., Liang, S. K., and Fan, W. X. (2015). The distribution characters of the stratospheric Brewer-Dobson circulation inferred from ERA-Interim. *Chinese J. Geophys.*, *58*(1), 20–31. https://doi.org/10.1002/cjg2.20152

Wei, K., Chen, W., and Huang, R. H. (2007). Association of tropical Pacific sea surface temperatures with the stratospheric Holton-Tan Oscillation in the Northern Hemisphere winter. *Geophys. Res. Lett.*, *34*(16), L16814. https://doi.org/10.1029/2007gl030478

White, I. P., Lu, H., Mitchell, N. J., and Phillips, T. (2015). Dynamical response to the QBO in the northern winter stratosphere: signatures in wave forcing and eddy fluxes of potential vorticity. *J. Atmos. Sci.*, *72*(12), 4487–4507. https://doi.org/10.1175/JAS-D-14-0358.1

Xie, F., Li, J. P., Tian, W. S., Feng, J., and Huo, Y. (2012). Signals of El Nino Modoki in the tropical tropopause layer and stratosphere. *Atmos. Chem. Phys.*, *12*(11), 5259–5273. https://doi.org/10.5194/acp-12-5259-2012